ELSEVIER

Composites Science and Technology 59 (1999) 179–200

COMPOSITES SCIENCE AND TECHNOLOGY

Mechanical performance of carbon-fibre- and glass-fibre-reinforced epoxy I-beams: III. Fatigue performance

M.D. Gilchrist [a,*], A.J. Kinloch [b], F.L. Matthews [c]

[a] *Mechanical Engineering Department, University College Dublin, Belfield, Dublin 4, Ireland*
[b] *Mechanical Engineering Department, Imperial College, Exhibition Road, London SW7 2BX, UK*
[c] *Centre for Composite Materials, Imperial College, Prince Consort Road, London SW7 2BY, UK*

Received 20 October 1997; received in revised form 16 February 1998; accepted 26 February 1998

Abstract

This paper is the third in a series which describe in detail the static and fatigue mechanical behaviour and fractographic observations of the failure of composite I-beams. Experimental investigations into the fatigue response of both unnotched and web- and flange-notched continuously reinforced carbon-fibre/epoxy and glass-fibre/epoxy I-beams are discussed in the present paper. A four-point flexural configuration was used to test the I-beams, each of which had the same multidirectional stacking sequence consisting of a balanced layup of 0, +45 and −45° plies. In no cases were the beams fatigued above the loads at which buckling of the compression flange would occur under static testing. The unnotched carbon/epoxy and glass/epoxy beams did not exhibit any detectable damage within 1.2×10^6 and 8×10^6 cycles, respectively. The notched beams, on the other hand, failed as a result of the tensile and compressive stresses which were present around the web notches. Damage mechanisms, including delamination, matrix microcracking and fibre fracture, were all present at final failure around the web notches, although the extent of the different mechanisms varied during the fatigue life of the I-beams.

Keywords: A. Polymer-matrix composites; B. Fracture; B. Fatigue; D. Optical microscopy; X-radiography

1. Introduction

It is becoming increasingly common for high-performance structural load-bearing components to be manufactured from composite materials. I-beams, based upon polymer matrix fibre-composites, have applications as support members in the wings of aircraft, tail-cones of helicopters, cores of rotor blades [1] and in civil engineering structures.

Varying degrees of tension and compression will exist in the flanges and shear in the web of such I-beams, depending on the attachments that are connected to the particular regions of a beam. Small degrees of torsion may also act along the length of an I-beam, although it is desirable to minimise this in practical situations because of the low torsional rigidity of such sections. The flanges may have an array of bolt holes for the attachment of panels or skins whilst the web region may have access holes for ducting or cables. Both types of hole will act as stress concentrators which can initiate damage and lead to component failure. Whilst laboratory tests attempt to simulate actual operating conditions, many simplifying assumptions and approximations to stress states and boundary conditions are often made both for convenience and in order to obtain results of more widespread and general applicability. For example, within shear tests [2], cantilever tests [3], three-point bending [4–7] and four-point flexure [8–11], the precise manner in which load is introduced into the test component may not truly represent the load distribution throughout a beam under the actual operating conditions. Also, in such experimental work it is often necessary to provide flange stiffeners to prevent buckling, or local reinforcements under the loading points to avoid premature failure in the loading regions, particularly when loading attachments may be drilled through the web of a beam and consequently may act as damage initiation sites. Similarly, the boundary conditions at the loading points [12–16] will influence the structural response of an I-beam. Thus, clearly the mechanical behaviour of any beam will be influenced by the various

* Corresponding author. Tel.: +353-1-7061890; fax: +353-1-2830534; e-mail: michael.gilchrist@ucd.ie

0266-3538/99/$—see front matter
PII: S0266-3538(98)00058-X

holes, attachments and stiffening stringers [4,7–21] which are associated with the component.

In addition to such geometric considerations, it is also important to consider the loading history to which a beam will be subjected. Whilst buckling can occur in composite structures it is rare for a composite member to be subjected to mechanical fatigue loads that would cause repeated buckling of the member, even though static failure of the same member could be initiated because of buckling [10]. In such instances, it may be necessary to stiffen a member artificially in order to raise the buckling load, prior to carrying out experimental fatigue tests, or, alternatively, to fatigue below the buckling loads of the component. For example, the static failure of E-glass/epoxy composite box-beams, tested under four-point flexure [8,9], has been found to lead to damage which is localised on the compressive face of the beam, close to one of the loading points. Carbon-fibre/thermoplastic-matrix composite I-beams, tested under three-point bending, failed in the compression flange [6], although this manner of failure was suppressed in further tests by using adhesively-bonded carbon-fibre/epoxy composite reinforcement caps. Failure in these components then occurred due to either shear failure of the web, or delamination of the tensile or compressive flange caps.

It is also possible to identify particular fractographic features of laminated composites which have been subjected to mechanical fatigue loads [22–28], although this is complicated by the inhomogeneities and anisotropy of the different materials systems. For example, fatigue striations have been identified on the imprints of fibres in mode II fatigue tests on a unidirectional laminate [23,24]. However, unlike in the fatigue of metals, it is not always possible to establish a relationship between their spacing and the remotely applied cyclic load [29]. The evolution of different forms of damage (e.g. fibre fracture, matrix cracking, fibre pull-out and delamination) during the fatigue life of a composite can be conveniently represented using damage mechanism maps [30,31]. These are S–N curves which identify the extent of different damage mechanisms present within a composite at different stages throughout its fatigue life. By representing damage in this manner, it is immediately clear which mechanisms are critical to the performance of a laminate.

The present paper discusses the mechanical response of unnotched carbon-fibre/epoxy and glass-fibre/epoxy I beams, as well as the behaviour of identical beams which contain a series of notches in the web and flange regions. The method of construction, from continuous prepreg tape, is outlined together with the four-point flexural testing arrangement. The response of the different beams to mechanical fatigue loads and the various damage mechanisms that occurred throughout the beams, at different stages in the loading history, are discussed in detail.

2. Experimental

2.1. Manufacture and testing of the I-beams

The authors have described the testing arrangement in greater detail elsewhere [10] and consequently will only summarise the salient points that are of immediate interest in the present paper. All the I-beams were manufactured using two preformed C sections and two flange caps, all of which were cured together in the same autoclave operation. The I-beams were of length 1200 mm, web depth 125 mm, flange width 75 mm and thickness 3 mm, as shown in Fig. 1. A 3 mm fillet radius was used at the web-flange junction; two spirally wound prepreg ropes (tows) were used to fill the triangular void which exists in this junction.

The stacking sequence was the same in the web and flanges of all the I-beams and contained a balanced, antisymmetric combination of $+45$, 0 and -45° plies, where the 0° direction is defined to be along the axis of the beam. Commercially available software [32] was used to design the beam stacking sequence such that there was a minimum number of coupling terms in the laminate stiffness matrix as well as the lowest possible interface moment, i.e. the τ_{zx} and σ_z stresses through the I-beam thickness were minimised. The actual (global) stacking sequence which was used is $(-45/0/+45^\circ)_{2s}$ $(+45/0/-45^\circ)_{2s}$, i.e.

$$-45/0/45/-45/0/45/45/0/-45/45/0/-45/45/0/-45/45/0/-45/-45/0/45/-45/0/45^\circ.$$

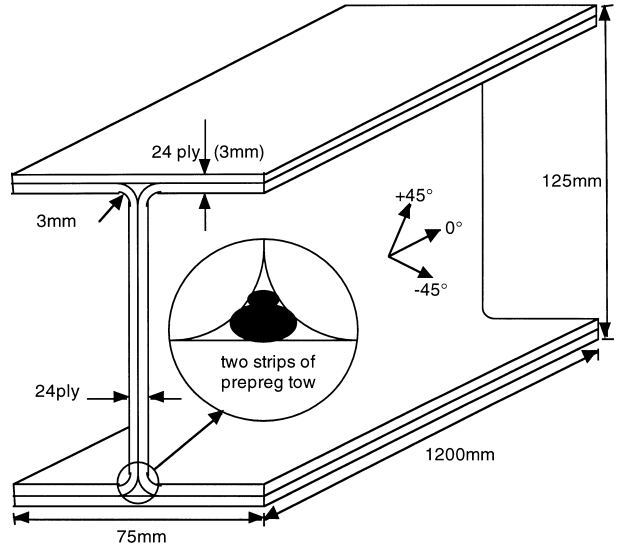

Fig. 1. I-beams are manufactured using two channel sections, two flange caps and strips of wound prepreg tow. The 24-ply layup has a $(-45/0/45^\circ)_{2s}(45/0/-45^\circ)_{2s}$ global stacking sequence, where the global 0° is along the axis of the I-beam as shown. The corresponding local co-ordinate system (not shown here) used for microscopy around web notches is $(0/-45/90^\circ)_{2s}(90/-45/0^\circ)_{2s}$ (cf. Figs. 2 and 7).

The mechanical properties of the carbon-fibre/epoxy [Ciba Composites (now Hexcel Composites) T300H/914] and glass-fibre/epoxy [Ciba Composites (now Hexcel Composites) E-glass/914] material systems were measured in accordance with the CRAG guidelines [33] and are given in Table 1. This table details both the unidirectional properties as well as those corresponding to the multidirectional stacking sequence that was used to manufacture the I-beams.

To test the I-beams, a four-point bending configuration was used with an arrangement of eight loading pads which were adhesively bonded to the web and undersides of the flanges as shown schematically in Fig. 2. A toughened epoxy adhesive (Permabond E38 using a room temperature cure and then post-curing at 50°C) was used initially, although this was found to fail during the first fatigue tests. In all subsequent tests a high-temperature cure adhesive (Permabond ESP 110 cured at 120°C) was used. One of each of the carbon/epoxy and glass/epoxy beams were fatigued in the virgin, unnotched, state. Both types of beams also had notches machined in the web and flange regions. The web notches usually consisted of two circular holes, of diameter 46 mm and 60 mm (i.e. some 40 and 50% of the internal web depth) located centrally in the two web regions between the sets of outer loading pads, where the shear is constant and at a maximum. A longitudinal array of six 5 mm diameter holes was also machined in both the tensile and compressive flanges of the web-notched beams, adjacent to the mid-length of the beams. No damage was evident around these latter notches and consequently they are not discussed any further in the present paper. All holes were machined by using diamond coated drills with sacrificial backing materials on both sides of the composite and this served to minimise the formation of damage (matrix cracking, splitting, surface deply, etc.) around the hole regions.

Load control on a servohydraulic machine was used for all the fatigue tests. A load ratio of $R=0.1$ was maintained for all the tests. This was done using the following procedure:

1. subjecting the components to a static load of $P_{\text{mean}}(=0.5(P_{\max}+P_{\min}))$ using a displacement mode of control;
2. changing the machine operating mode from displacement control to load control;
3. increasing the amplitude of the fluctuating load until the actuator ranged from $P_{\min}$ to $P_{\max}$, after which stage the cycle counter was switched on;

Table 1
Measured mechanical properties of unidirectional and multidirectional carbon/epoxy and glass/epoxy composites

Property	Carbon/epoxy (T300/914)		Glass/epoxy (E-glass/914)	
	Unidirectional	Multidirectional	Unidirectional	Multidirectional
E_{11}, (GPa)	134.75	54.75	45.37	26.68
E_{22}, (GPa)	8.24	21.98	15.20	16.94
ν_{12}	0.325	0.704	0.289	0.477
ν_{21}	0.012	0.287	0.074	0.291
X_{Lten}, (MPa)	1563.00	534.20	1049.00	432.77
X_{Tten}, (MPa)	44.76	277.12	46.48	220.45
G_{12}, (GPa)	Not measured	–	6.03	–

The stacking sequence used for the multidirectional laminates was the same as that used to manufacture the I-beams, namely $(-45/0/45°)_{2s}(45/0/-45°)_{2s}$. Note that no shear modulus has been measured for the multidirectional stacking sequence: this is in agreement with the CRAG [33] guidelines.

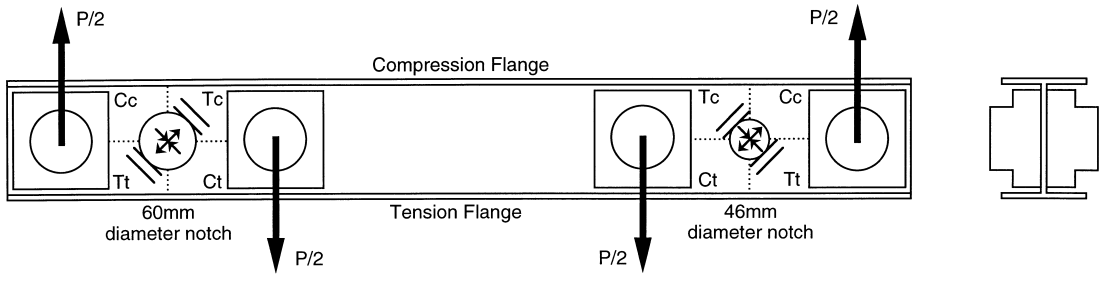

Fig. 2. Schematic diagram of the four-point flexure loading arrangement used for static and fatigue tests of I-beams. The shear stress around the web notches can be resolved into direct tensile and compressive stresses which act in four different quadrants, Tt, Tc, Cc and Ct, as shown. Quadrants Tt and Tc are subject to a resolved tensile stress state and Cc and Ct to a resolved compressive stress state. Quadrants Tt and Ct are adjacent to the tension flange whilst Tc and Cc are adjacent to the compression flange. Sections for optical microscopy were taken after testing from around the web notches, typically in quadrants Tt and Tc. Such sections were parallel to the global ±45° orientation (cf. Figs. 1 and 7).

4. setting displacement trips to interrupt the test if there was a certain percentage reduction in the global stiffness of the beam; and
5. setting cycle counter trips to halt the test after a certain number of fatigue cycles.

The displacement trips were set such that the test would interrupt upon a specified global increase in compliance (typically 5–10%) whereas the cycle counter trips were set for different numbers of fatigue cycles (typically 10^5–10^6 cycles). It has been observed during tension fatigue tests [30,31] and compression fatigue tests [34–36] that, following a relatively rapid initial drop in stiffness, there is a gradual reduction in stiffness over a large number of fatigue cycles prior to a final large drop in stiffness and failure over relatively few loading cycles. However, this was not generally observed during the present fatigue tests for reasons that were thought to be due to the test arrangement. Namely, each beam was tested in blocks of fatigue cycles, between which the beams were non-destructively tested to quantify the extent of any damage. A global reduction (of the order of 5–10%) in the stiffness of the I-beams was observed during each successive block of fatigue cycles. It was thought that this was associated with 'bedding-in' and wear of bearings, and loading attachments, in the test arrangement, rather than damage within the components. The frequency of testing used was 5 Hz and 1 Hz for the carbon-fibre and glass-fibre I-beams, respectively.

The damage that was identified throughout the flange and web areas of the beams after each block of fatigue cycles was assessed using a wide range of techniques, although not every technique was used for each beam. Having assessed the extent of damage in the components, the I-beams were replaced in the testing machine and the fatigue test restarted and continued. The non-destructive and destructive techniques that were used are discussed below.

2.2. Non-destructive inspection techniques

2.2.1. Edge replication

Edge replication is an inexpensive and quick technique which proved convenient for non-destructively determining the presence of damage on an edge of a specimen, such as the edge of a compression flange of an I-beam or the circumference of a web notch. In order that different mechanisms of damage could be detected, it was first necessary to polish the specimen edge to a level that was suitable for optical microscopy (i.e. a 6 μm polish, or finer). This proved to be easier to achieve on flat edges, such as the edge of a compression flange, than on a curved edge, such as the circumference of the web notches. Nevertheless, in some of the fatigue tests on the notched carbon/epoxy I-beams, it was possible to create damage mechanism maps which identified that matrix cracks and delaminations occurred at particular regions around the circumference of the web notches early in the fatigue life of the components (e.g. within 10 000 cycles). Thus it was possible to establish which plies developed matrix cracks and along which ply interfaces any delaminations occurred. This technique, being a surface assessment technique, was not able to identify damage away from free surfaces. However, Chen et al. [30,31] have suggested that such information would be indicative of the radial damage away from the notches within the various plies. Within the I-beams of the present work, it was found that the extent of matrix cracking and delamination around the circumference of the holes which was identified relatively early in the tests did increase slightly with the number of fatigue cycles as the tests progressed.

2.2.2. Ultrasonic scanning

All flange and web regions of the unnotched and notched I-beams were ultrasonically scanned at each interruption of the fatigue tests. In some cases, this meant that a beam was scanned up to ten times during a given fatigue test. All I-beams were C-scanned prior to testing in order that the subsequent development of any damage would be accurately determined. During the fatigue tests of the notched I-beams, when it became apparent that damage was localised around the large web notch, it was possible to use a portable ultrasonic scanner without having to remove the component from the testing machine. However, it was generally difficult to scan an area with complete consistency using this method and, consequently, this portable scanner did not fully replace the use of the more conventional C-scanner, which involved removing the I-beam from the testing machine and automatically scanning the beam in an immersion tank.

It was often useful to consider the A-scans of particular regions of the I-beams since these would reveal those ply interfaces which had delaminated. This was particularly true for the static tests [11]. However, this method was found to be less useful for the fatigue tests, since delamination was less extensive than in the static tests. Around the web notches in the fatigue tests it was possible to ascertain that damage mechanisms other than solely delamination were occurring; this was clear from the multiple reflections identified in the A-scan. However, since such damage was generally close to the edge of the notch, it was difficult to define the extent of this given the relatively large spot-size of the ultrasonic transducer. Consequently, it was necessary to use other damage assessment techniques, in conjunction with the ultrasonic methods.

2.2.3. Thermographic and photoelastic methods

Thermography and photoelasticity were also used in an attempt to provide additional information on the

initiation and development of the different damage mechanisms which developed during the fatigue tests.

Since it was known that failure of the notched I-beams was localised around the web notches, it was convenient to focus a thermal imaging infra-red camera on this complete web region during the fatigue tests. It was possible to do this without interrupting the tests, although a better degree of resolution was obtained by stopping the machine actuator and holding a specimen under the mean load, P_{mean}, whilst recording the thermal image. The resolution of the infra-red camera was such that it was possible to determine temperature differences of 0.2°C. This proved sufficient to establish that the temperature rise due to damage, and not to autogeneous heating of the matrix (since the loading frequency did not exceed 5 Hz), was greatest around the circumference of the notch. However, it was not possible to ascertain the area of damage with the same degree of accuracy as was provided by employing the ultrasonic methods. It was also noted that there was less certainty associated with the thermal images from the carbon/epoxy I-beams than with the glass/epoxy I-beams. It is believed that this was due to the higher thermal conductivity of the carbon fibres than that of the glass fibres.

Photoelastic epoxy coatings, of different thicknesses and strain sensitivities, were used in an attempt to establish full-field information on the initiation and development of damage around the web notches during the fatigue tests. Various coatings, with appropriately sized pre-machined holes, were bonded to the web around the larger notch. Isochromatic fringe patterns were clearly evident under static conditions up to P_{mean}, with greater levels of strain being evident up to P_{max}. Such fringes were also noted by Kemmochi and Uemura [37] during static tests on sandwich beams. Fringes were also apparent during the fatigue tests, although it was convenient to interrupt a fatigue test and hold the I-beam under the mean load to capture the distribution of strain fringes. However, the coating material that provided a sufficient resolution of the strains throughout the web region began to crack after just a few thousands of fatigue cycles, and was therefore unsuitable for subsequently assessing the distribution of strains throughout the web region of the I-beam. The regions of coating material that cracked were identical to those quadrants of the notched web that were subjected to direct tensile stresses (arising, of course, from the resolved shear stresses). The photoelastic coatings were polycarbonate (Measurements Group PS1) with a medium degree of strain sensitivity and these had been bonded to the surfaces of the I-beams using epoxy adhesive (Measurements Group PC6). While a coating of lower strain sensitivity would be less likely to crack, it would not provide a sufficient number of photoelastic fringes under the applied loads to obtain highly accurate estimates of surface strain gradients.

Thus, the thermographic and photoelastic methods were found to be of rather limited use in the present work.

2.3. Destructive inspection techniques

Dye-penetrant enhanced X-radiography, optical and scanning electron microscopy were variously used to assess the damage in the I-beams after each fatigue test was fully completed. These were particularly useful in quantifying the extent and mechanisms of damage in regions that had previously been identified, via the non-destructive techniques described above, as containing damage.

Zinc iodide and dibromomethane were both used as dye-penetrants for X-radiography. Details of the precise conditions of use have already been given by the authors [11]. Whilst it would have been possible to X-ray particular regions of the I-beams, such as around the web notches, at intervals during fatigue tests, this was not done, principally because of the possibility of the dye-penetrant degrading the epoxy matrix of the composite. There were also physical limits to the size of a component which could fit within the X-ray chamber that was used during the project. However, as a post-failure analysis technique, X-radiography provided excellent two-dimensional information on the extent and mechanisms of fatigue damage that existed around the web notches.

It was also necessary to obtain through-thickness information on damage around the web notches, in addition to the two-dimensional information provided by X-radiography. This was readily provided by optical microscopy of sections taken through the thickness of the I-beams, after the damage had been located accurately using radiography. Thus, it was possible to establish the density of matrix cracking around the notches in the web and in the various plies through the laminate thickness, the presence of fibre fracture and inter-ply delaminations. It was also possible to quantify the development of such damage with increasing number of fatigue cycles, since a number of I-beams were tested under identical load conditions but cycling was stopped, and the beam cut into specimens for the microscopy studies, after varying numbers of fatigue cycles had been reached.

3. Behaviour of I-beams under mechanical fatigue loads

3.1. Introduction

A range of fatigue loads was applied to the four different types of I-beam; in all cases, however, the maximum load levels were not sufficient to cause any

detectable measure of buckling either on the compression flange or in the web regions. Typically, the maximum levels of the load in the fatigue tests were 90% of those loads which were required to cause global buckling of the compression flange. The static failure of the I-beams associated with such buckling has been reported elsewhere [10] and, consequently, will not be discussed here. The maximum levels of fatigue load in the unnotched and notched carbon/epoxy and E-glass/epoxy I-beam fatigue tests were approximately 50 and 65%, respectively of the static strengths.

No clear evidence of fatigue damage was observed in the unnotched I-beams. Within the notched I-beams, on the other hand, both tensile and compressive damage were observed but were localised around the web notches in the form of matrix cracking, fibre fracture, fibre buckling and delamination. No global buckling was observed although, following the initiation of delamination around the web notch in the E-glass/epoxy I-beam, local buckling did occur with the delamination visibly opening and closing during each fatigue cycle. The fatigue test conditions, and assessment of the damage initiation site, for the beams are given in Table 2. The general features of damage that were identified in the various beam tests are discussed in the following sections, and these are then assessed and discussed with respect to damage evolution and fatigue life in Section 4.

3.2. Fatigue failure of unnotched I-beams

Table 3 summarises the results from the three unnotched I-beams that were tested under fatigue conditions. The first I-beam to be tested was an unnotched carbon/epoxy I-beam (termed Carbon U1) that was identical in all respects to the beams that had been tested statically [10]. Now, for the static tests on the carbon/epoxy I-beams, flange buckling occurred at a load of 55 kN. Therefore, it was decided to set the maximum fatigue load at some 75% of this buckling load, i.e. to test between 4–40 kN. (It was considered not to be realistic to fatigue above the buckling load, since such conditions would seldom occur under normal operating conditions.) This maximum fatigue load was approximately 40% of the ultimate failure load of 96 kN. No evidence of damage was observed after cycling for 1.2×10^6 cycles in this I-beam using the various non-destructive techniques.

Consequently, in an attempt to induce some structural damage, it was decided to stiffen the flanges of the above carbon/epoxy I-beam (i.e. the Carbon U1 beam) with mild steel stringers and to fatigue the same beam between 10 and 100 kN while raising the buckling load above 100 kN. While this could have been done by adding additional unidirectional plies to the flanges, either at the manufacturing stage or in a subsequent operation, it was more convenient to use a high modulus material which had a relatively small cross-section. A square cross-section bar (6 mm×6 mm) was bonded to the opposite surfaces of the edges of both the tensile and compressive flanges. However, it was recognised that this I-beam would now not be subjected to the same strains as were suffered by the I-beams used in the previous static tests. For example, the maximum strain on the compression flange of the stiffened I-beam was only 0.25% at the maximum fatigue load of 100 kN, compared with a strain of some 0.84% at a similar actuator load during the static test on the unstiffened I-beam. A second I-beam (termed Carbon U2) was similarly modified by bonding on stiffners and subjected to fatigue testing in an identical manner. However, these flange-stiffened carbon/epoxy I-beam tests were unsuccessful in

Table 2
Summary of fatigue test conditions of the carbon/epoxy and glass/epoxy I-beams

	Carbon/epoxy		Glass/epoxy	
	Unnotched	Notched	Unnotched	Notched
Load range	various	5–50 kN	3.5–35 kN	3.5–35 kN
Damage initiation site	No damage evident up to 1.2×10^6 cycles	At web notch	No damage evident up to 8×10^6 cycles	At web notch

Table 3
Unnotched I-beam fatigue tests

Beam	Summary of results
Carbon U1	4–40 kN for 1.2 M cycles. No evidence of any damage.
Carbon U1 (re-used)	Eight adhesively-bonded flange stiffeners added. 10–100 kN for 47 k cycle, then failure occurred around the flange stiffeners.
Carbon U2	Eight adhesively-bonded flange stiffeners added. 10–100 kN for $\approx$5000 cycles, then failure associated with debonding of the flange stiffeners.
Glass U1	3.5–35 kN for 8 M cycles. No evidence of any damage.

that damage of the I-beam initiated from (i) around the flange stiffeners, or (ii) around the loading pads, or (iii) via debonding of the loading pads, or (iv) debonding of the flange stiffeners; rather than being exclusively contained within the composite I-beam itself. These unrepresentative types of failure occurred within 10^5 cycles.

A single unnotched glass/epoxy I-beam (termed Glass U1) was also tested under fatigue conditions, but without any additional flange-stringers such as had been used on the carbon/epoxy beams. The actuator load range was from 3.5 to 35 kN; this maximum load of 35 kN corresponded to the onset of buckling of the compressive flange during the static test. The maximum load was almost 50% of the failure load of the statically-tested unnotched glass/epoxy I-beam. A frequency of 1 Hz was used during the fatigue test and after some 8.0×10^6 cycles the test was interrupted. No fatigue damage was detected in either the beam or the loading attachments.

Since no fatigue damage was detectable at all in the composite materials themselves, either for the carbon/epoxy I-beam (after testing for 1.2×10^6 cycles) or the glass/epoxy I-beam (after testing for 8×10^6 cycles), it was decided to notch the I-beams before conducting any further tests.

3.3. Fatigue failure of notched I-beams

3.3.1. Carbon/epoxy beams

3.3.1.1. Introduction. Five notched carbon/epoxy I-beams were tested under a fatigue range of 5–50 kN. This maximum load of 50 kN for the fatigue cycle represented about 90% of the 55 kN associated with the onset of buckling in the compressive flange, as was observed for the static testing of the notched carbon/epoxy I-beams [10]. The reason that 55 kN was used for these notched I-beam fatigue tests, as opposed to the 40 kN used for the unnotched beams, was that the preliminary tests had indicated that the I-beams possessed excellent fatigue behaviour. Thus, to obtain fatigue failures in a reasonable timescale, apart from introducing notches into the beams, it was also decided to increase the maximum load for the fatigue cycle to a level which did not exceed the buckling load for the beams. The notched glass/epoxy I-beams, on the other hand, were even more tolerant of fatigue damage because of the higher failure strains of the glass fibres. Consequently, it was decided that the maximum load for the fatigue cycle of these beams should be raised to 35 kN, i.e. 100% of the load associated with the onset of buckling in the compressive flange which had been established when testing the notched glass/epoxy I-beams under static conditions [10]. The details of the five notched carbon/epoxy tests are summarised in Table 4. Apart from one preliminary test (Carbon N1) only one of these beams (Carbon N5) failed after fatigue testing; all the other tests were halted prior to fracture.

3.3.1.2. Preliminary tests on Carbon N1 beam. One preliminary I-beam (termed Carbon N1) had a circular notch and a diamond notch in the two shear-loaded web-regions. The diameter of the circular hole was 46 mm whilst the maximum dimension of the diamond hole was also 46 mm. It has been noted elsewhere [38] that circular holes are weaker under static shear conditions than diamond holes. This was also the case for this preliminary fatigue test which lasted for 5.09×10^6 cycles, after which the test was stopped and the specimen was examined to assess the extent of damage. Edge replicates had previously been taken around the

Table 4
Notched I-beam fatigue tests, including damage detection methods employed

Beam	Summary of results
Carbon N1	5–50 kN for 5.09 M cycles. Test stopped due to failure of adhesive under loading pads. Diamond and small circular notches (46 mm diameter); edge replication of damage around circular notch at different numbers of cycles (0.54, 1, 1.48, 2.04, 2.1, 2.46, and 5.09×10^6 cycles); ultrasonic scans at different numbers of cycles (0, 0.54, 0.66, 0.84, 1.0, 1.48, 2.0, 2.04, 2.46, and 5.09×10^6 cycles).
Carbon N2	5–50 kN for 0.5×10^6 cycles. Circular notches (46 mm and 60 mm diameter) machined in web of beam. Some damage around large notch; test was interrupted prior to failure; X-ray and optical through-thickness views of damage at end of test.
Carbon N3	5–50 kN for 2.43×10^6 cycles. Circular notches (46 mm and 60 mm diameter) machined in web of beam. Photoelastic coating cracked early in test; test was interrupted prior to failure.
Carbon N4	5–50 kN for 4.5×10^6 cycles. Circular notches (46 mm and 60 mm diameter) machined in web of beam. Some damage; X-ray, ultrasonic C-scan and optical through-thickness views of damage at end of test; test was interrupted prior to failure.
Carbon N5	5–50 kN for 4.78×10^6 cycles. Circular notches (46 mm and 60 mm diameter) machined in web of beam. Failure was localised around large notch; X-ray and optical through-thickness views of damage at failure.
Glass N1	3.5–35 kN for 0.96×10^6 cycles; some damage around large notch; X-ray, ultrasonic C-scan and optical thro-thickness views of damage at end of test; test was interrupted prior to failure.
Glass N2	3.5–35 kN for 3.11×10^6 cycles; photoelastic coatings were adhesively bonded around large web notch; damage was masked by photoelastic coatings and could not be assessed optically; test was interrupted prior to failure. SEM after testing was unsuccessful.

circumference of the circular notch at 0.54×10^6 cycles and at five other intermediate intervals before the final 5.09×10^6 cycles. Ultrasonic C-scans were also taken of every region of the I-beam at the same intervals. The ultrasonic scans, shown schematically in Fig. 3, revealed that damage growth occurred around the circular notch within the first loading interval, i.e. within 0.54×10^6 cycles, and that the damage continued to develop, albeit at a slower rate, until the test was stopped. The damage was principally confined to the edges of the notch that were in the four quadrants of the web region; i.e. those quadrants that were subjected to resolved tension and compression and were adjacent to the tension and compression flanges. Machining damage (caused by breakthrough of the cutter to the back face of the web) was identified only around the diamond hole, but no development of this was detected during the fatigue test. The edge replicates around the circular notch showed clear indications of matrix cracking in plies of all orientations, and delaminations along interfaces of 45 and 90° relative orientations (i.e. between the 0/45° and the +45/−45° plies). Fig. 4 identifies the typical distribution of damage observed around the inner circumference of the hole, or notch, when using the edge replication method. The density of damage was different in each ply and this is discussed in greater detail in the following section. The damage, however, was clearly evident after 1×10^6 cycles and much of this damage was apparent after 0.54×10^6 cycles. After 5.09×10^6 cycles this damage did not appear to be more extensive around the circumference of the hole. Neither did there appear to be a significantly greater density of matrix cracking or delamination at the end of the test than earlier in the test. This evidence would suggest that the fatigue damage occurred rapidly during the early stages of the test and any subsequent development of this damage was at a much slower rate of propagation. These edge replicates did not provide any indication of the damage away from the edge of the notch, whereas the ultrasonic scans identified broad regions of damage away from the edge of the circular notch. The resolution of the C-scans, however, was inadequate to detect any possible matrix cracks that might have been present more than 5 mm away from the edge of the notch. Neither was it possible to resolve between delamination and a high density of matrix cracking using the ultrasonic methods, since the location of the damage was too close to the edge of the notch.

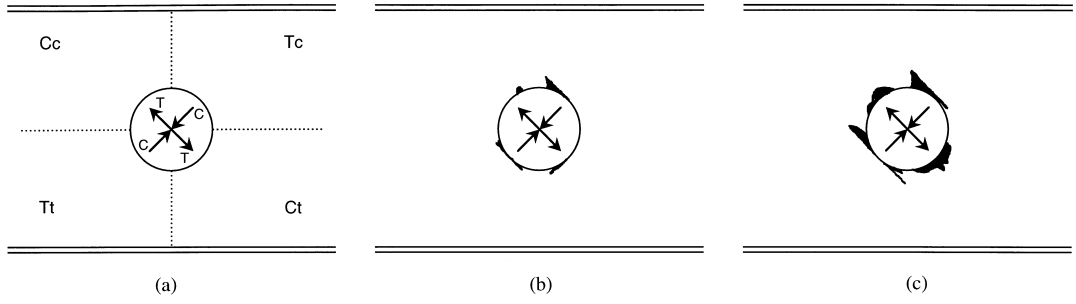

Fig. 3. Schematic of ultrasonic C-scans to identify the development of fatigue damage around the small circular notch (46 mm diameter) in the web of beam Carbon N1 (a) prior to testing, (b) after 0.54×10^6 cycles and (c) after 5.09×10^6 cycles. [The directions of resolved tensile (T) and compressive (C) stresses that act in the four different quadrants around the web notch are identified in (a), and are identical in (b) and (c).] The compressive flange is at the top and the tensile flange is at the bottom of the diagram.

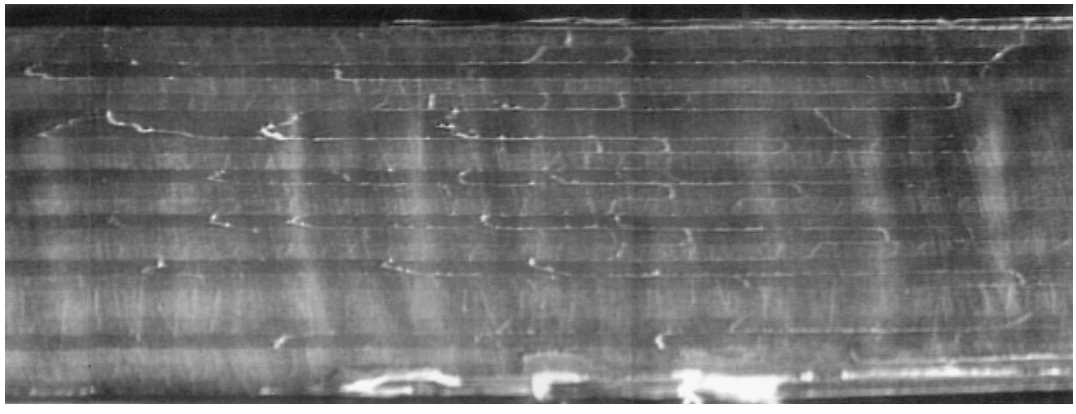

Fig. 4. Edge replication which identifies through-thickness matrix cracking and delamination around the circumference of the circular notch in quadrant Tt of beam Carbon N1 after 2×10^6 cycles. The thickness of this section is 3 mm (= 24 plies).

3.3.1.3. Tests on Carbon N2 to Carbon N5 beams. The remaining four carbon/epoxy I-beams were notched with circular holes and were subjected to an identical loading range of 5–50 kN. The circular notches were 46 mm and 60 mm in diameter and were located centrally in the web regions. The larger notch was machined in the I-beam, instead of the diamond notch, and it was around this notch that failure and damage were concentrated, although damage was also noted around the smaller hole. The beams were tested for 0.5×10^6, 2.43×10^6, 4.5×10^6 and 4.78×10^6 cycles. The 4.78×10^6 cycle test showed complete failure of the web region due finally to fibre fracture, whilst the other three beam tests were stopped after different numbers of fatigue cycles before failure in order to ascertain the rate of development of the different fatigue damage mechanisms.

The damage around the holes of these four notched carbon/epoxy I-beams was induced by both local tensile and compressive stresses, which arose due to the distribution of the shear stresses around the web notch. The tensile-induced damage was considered to be catastrophic in the sense that it was this damage which extended to both the top and bottom flanges, and was responsible for the eventual loss of structural integrity of the I-beam. The compressive-induced damage, on the other hand, was essentially located in one quadrant of the web but covered a larger proportion of web area than the tensile damage. This is most likely due to the buckling which was observed to be located about edge delaminations which were present in the compressive region of the notch.

The damage in the tensile quadrants was considerably cleaner and sharper in appearance than damage induced by the compressive stresses, and Fig. 5 schematically represents the evolution of damage around the large hole, as detected using ultrasonic C-scanning. The detail in these diagrams only indicates different levels of attenuation of ultrasonic signal and the authors have not attempted to correlate attenuation with different damage mechanisms [39]. Examining the ultrasonic A-scan of the compressive damage around the web notch [see Fig. 5(c)], indicates that this consists of multiple delaminations. These were also identified subsequently in the microscopic analysis of the through-thickness distribution of damage and the edge replicates, as shown in Fig. 4. The ultrasonic probe spot-size, however, was not of sufficient accuracy to establish the exact nature of the tensile-induced damage around the notch.

Examination of the X-radiographs was particularly informative, especially when considered in conjunction with the results from the ultrasonic scanning methods. X-radiographs, taken at the end of the test, around the large web notches in beams Carbon N2 (0.5×10^6 cycles), Carbon N4 (4.5×10^6 cycles) and Carbon N5 (4.78×10^6 cycles) and the small web notch in beam Carbon N5 are detailed in Fig. 6. (Note that in Fig. 6(b), (c) and (d), the strain gauges which were bonded onto the I-beams may be seen.) X-rays were taken ($\approx$20 kV for 5 mins at 3 mA) using both dibromomethane and zinc iodide as the dye penetrants. Whilst the former penetrant did not leave a saline residue on the fracture surface, it did not identify as much damage as the zinc iodide. A saline residue can mask the fractographic features from view during subsequent SEM investigations and, consequently, dibromomethane was used during most of this project. Fig. 6(c) shows the fracture around the large web notch after failure of beam Carbon N5 and reveals almost too much damage to be particularly informative since it is not immediately clear which damage mechanisms are the more critical. The compressive damage is particularly extensive and appears in the form of major delaminations with some matrix cracking being visible, although this is completely within the boundary of the delamination area. Similarly, the tensile damage appears to extend as a clean fracture from areas round the edge of the notch which contain matrix cracks. However, the radiographs of the small notch Fig. 6(d), and the large notches in the beams which did not fail [Fig. 6(a) and (b)] are more informative. These identify a dense concentration of matrix cracks in the 0, +45 and −45° plies, very close to the

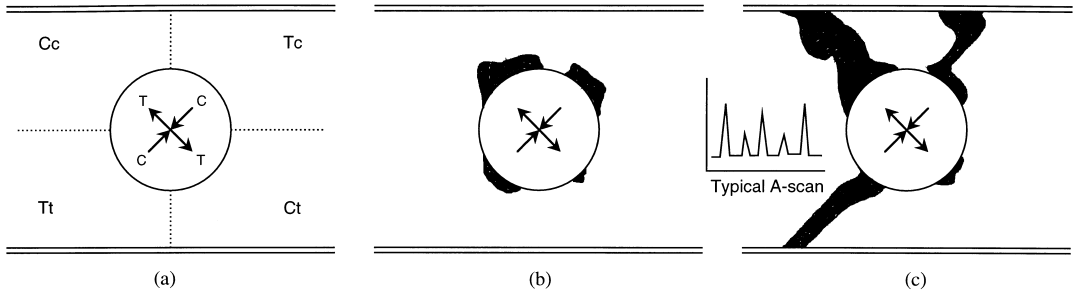

Fig. 5. Extent of damage around the large web notch (60 mm diameter) of beam Carbon N5 as detected using ultrasonic C-scan after (a) 0.74×10^6 cycles, (b) 4.68×10^6 cycles and (c) 4.78×10^6 cycles, i.e. failure. The orientation of each scan is identical. A typical A-scan from quadrant Cc is shown in (c); delaminations are present in this instance at two locations in addition to the midplane, as can be inferred from the oscilliscope image of the front, back surface and intermediate reflections.

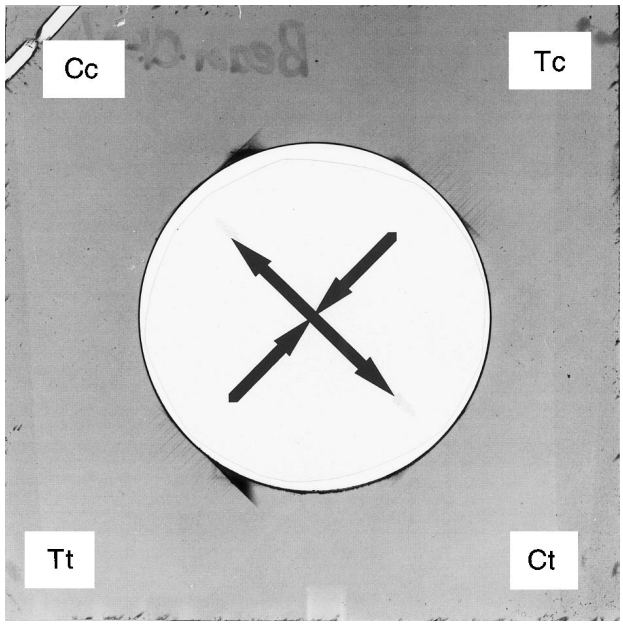

Fig. 6. (a) X-ray radiograph of fatigue damage around 60 mm diameter notch in beam Carbon N2 (0.5×10^6 cycles). Tensile matrix cracks are evident in quadrants Tc and Tt (top right and bottom left, respectively) spanning a width of some 20 mm for a distance of up to 6 mm away from the edge of the notch. The compression flange is along the top of the photograph and the tension flange along the bottom. The local directions of resolved tensile and compressive stresses are indicated.

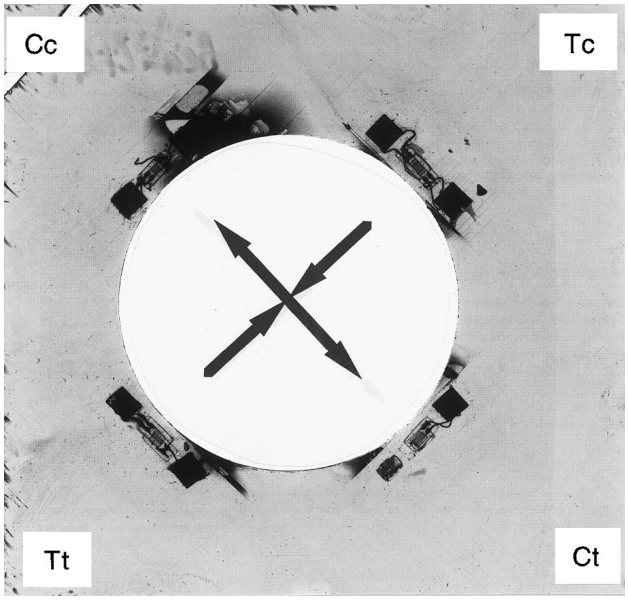

Fig. 6. (b) X-ray radiograph of fatigue damage around 60 mm diameter notch in beam Carbon N4 (4.5×10^6 cycles). Tensile matrix cracks are evident in quadrants Tc and Tt (top right and bottom left, respectively) spanning a width of some 27 mm for a distance of approximately 8 mm away from the edge of the notch. Delamination is greater in quadrant Cc ($\approx30\times10\,mm^2$) than in quadrant Ct. The compression flange is along the top of the photograph and the tension flange along the bottom. The local directions of resolved tensile and compressive stresses are indicated.

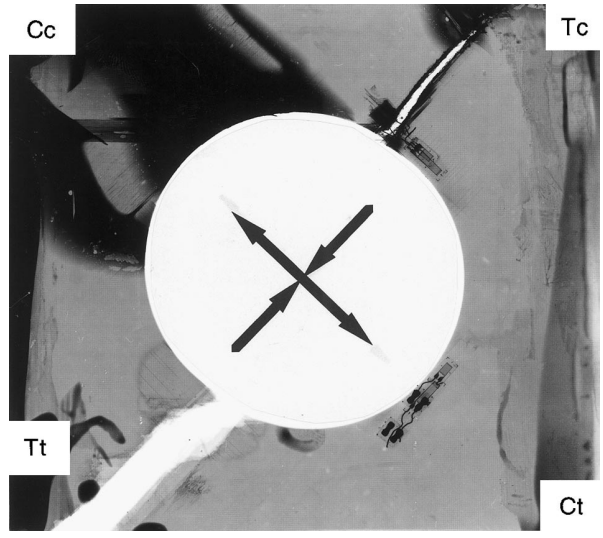

Fig. 6. (c) X-ray radiograph of fatigue damage around 60 mm diameter notch in beam Carbon N5 (4.78×10^6 cycles). The web section has completely fractured due to the local tensile stresses in quadrants Tt and Tc (fracture spans bottom left and top right quadrants). The damage in quadrant Tt (bottom left) has more clearly propagated to the tension flange than in quadrant Tc, where some few plies have not completely fractured close to the compression flange. There is extensive delamination in quadrant Cc (top left) but none in quadrant Ct. The width of this delamination is approximately equal to the diameter of the notch and it extends directly to the compression flange. The compression flange is along the top of the photograph and the tension flange along the bottom. The local directions of resolved tensile and compressive stresses are indicated.

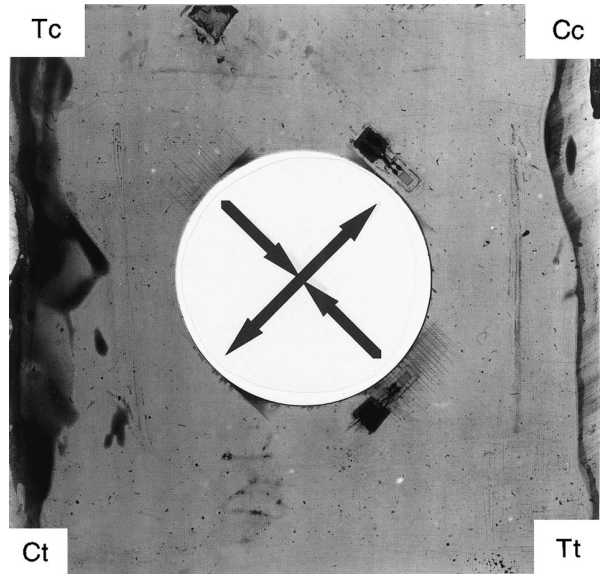

Fig. 6. (d) X-ray radiograph of fatigue damage around 46 mm diameter notch in beam Carbon N5 (4.78×10^6 cycles). Tensile matrix cracks are evident in quadrants Tc and Tt (top left and bottom right, respectively) for a distance of up to 10 mm away from the edge of the notch. The compression flange is along the top of the photograph and the tension flange along the bottom. This notch was at the opposite end of the I-beam to the notch of Fig. 6(c) and consequently the local directions of resolved tensile and compressive stresses appear to act in opposite directions to those shown in Fig. 6(c).

free edges of the holes; and it appears that the matrix cracks within the plies which are aligned orthogonally to the tensile forces are the most extensive around the notches.

Edge replication was used at certain intervals of cycling during some fatigue tests to identify the damage around the circumference of the large notch. The density, distribution and mechanisms of damage that were identified are very similar to those observed around the small hole, as shown in Fig. 4. Similar information is provided at failure by using optical microscopy to examine polished sections at different distances ahead of the notch, as typically shown in the micrograph of Fig. 7. In this manner it is possible to establish the

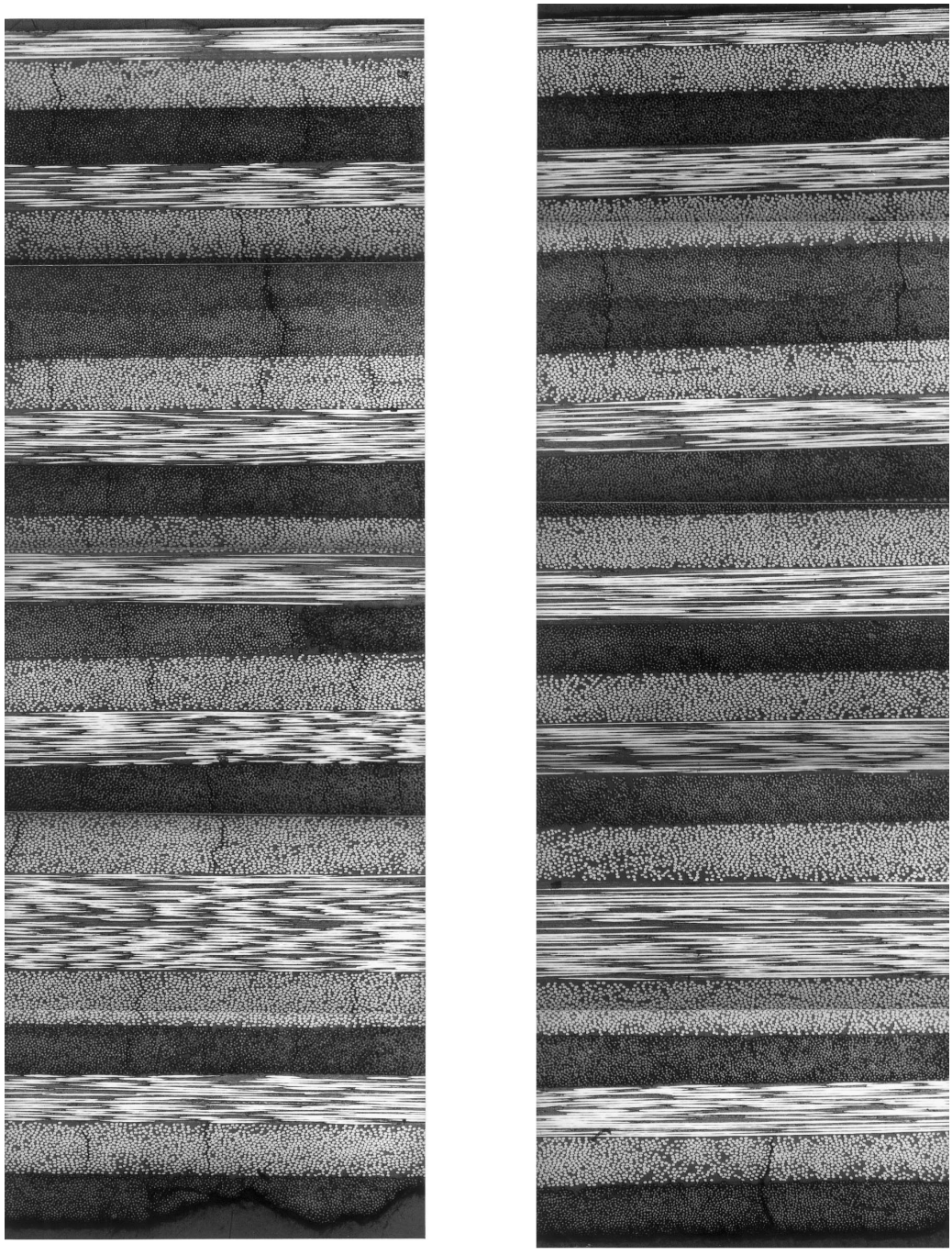

Fig. 7. Optical micrograph of through-thickness damage around the small notch of beam Carbon N2 (0.5×10^6 cycles) taken after test (a) at edge of small notch and (b) 6.5 mm ahead of the small notch. Note that the local orientation of the plies in these micrographs is $(0/-45/90°)_{2s}(90/-45/0°)_{2s}$ whilst the global orientation of these same plies is $(-45/0/45°)_{2s}(45/0/-45°)_{2s}$. This is because the sections were cut normal to the direct tensile stresses within quadrant Tt and this orientation is parallel to the global 45° direction (cf. Figs. 1 and 2).

density of matrix cracks (and any other damage mechanisms) in terms of both loading cycles and distance away from the free edge of a notch. The optical micrographs of Fig. 7 have been taken from two different positions in the vicinity of the small hole (46 mm diameter) of beam Carbon N2. The first section [Fig. 7(a)] is tangential to the edge of the hole whilst the second section [Fig. 7(b)] is parallel to the first but some 6.5 mm away from the edge of the hole. Both sections are in the tensile quadrant that is adjacent to the tensile flange of the beam. It should be noted that the local orientation in which these micrographs have been cut is different from the global coordinate system of the I-beams [i.e. the local orientation in Fig. 7 is (0/45/90°) whilst the global orientation is (−45/0/+45°)]. Matrix cracks are evident at the edge of the hole [Fig. 7(a)] in all local 45 and 90° plies but at some 6.5 mm away from the edge of the hole [Fig. 7(b)] matrix cracks are only evident in the local double 90° plies. Some cutting damage, due to back surface breakout of the diamond cutter, is apparent in the bottom ply at the edge of the hole.

3.3.1.4. Discussion of failed beam (Carbon N5). The visual damage after failure around the large hole of beam Carbon N5 is shown in Fig. 8. The crack which had developed, completely through the thickness of the composite, at right angles to the local direction of the tensile stresses, may be clearly seen; especially from the photograph of the front face. Indeed, the crack has grown through the web until it meets the compression and tension flanges.

However, the extent of the actual damage is shown more clearly in the ultrasonic C-scans of Fig. 5 and the X-ray radiograph of Fig. 6(c). These studies reveal that the integrity of the I-beam is lost due to the fracturing (i.e. matrix cracking, transverse splitting and fibre fracture) of the web region into two halves. The compressively loaded region can sustain some residual load, unlike the tensile region, which has fractured completely between the top and bottom flanges. The extent of the damage associated with this tensile fracture is not as large as the compressive damage. This is quantifiable by observing that the width of tensile damage is of the same order of magnitude as the thickness of the I-beams, whilst the width of compressive damage is of the same order of magnitude as the diameter of the notch. It is believed that matrix cracks, close to the stress concentration around the notch, propagated towards the flanges, and that this eventually led to fibre fracture and structural failure of the I-beams.

3.3.2. Glass/epoxy I-beams

Two notched glass/epoxy I-beams were tested under a fatigue load range of 3.5–35 kN, as noted in Table 4. The web notches were identical to those machined in the carbon/epoxy beams, i.e. 46 and 60 mm diameter. Local buckling of the web was observed during tests on these glass beams, when delamination was also present around the large web notch. The first of these I-beams (Glass N1) was tested for 0.96×10^6 cycles and the damage around the web notches has been examined by visual observation, X-radiography, ultrasonic C-scanning and through-thickness optical microscopy.

The second glass/epoxy beam (Glass N2) was tested for 3.11×10^6 cycles. A variety of photoelastic coatings were bonded to the web regions around the large notch and, after testing, this region of the beam was sectioned for examination using scanning electron microscopy. The strain fringes were evident in all three photoelastic

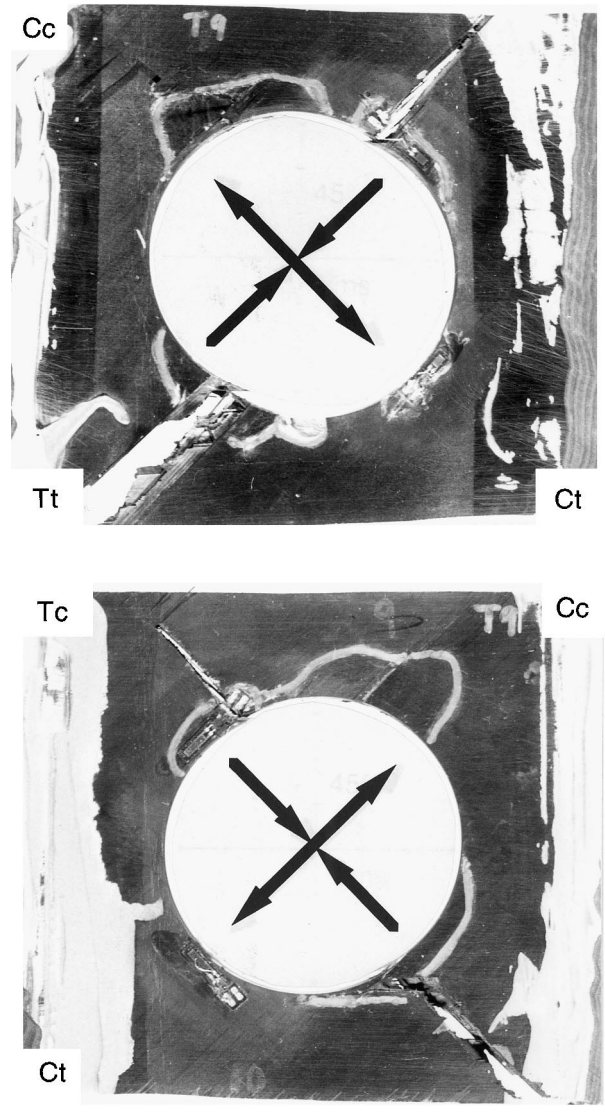

Fig. 8. Visually identified damage after failure around the front and back of the large web notch (60 mm diameter) in beam Carbon N5. The compression flange is along the top of the photograph and the tension flange is along the bottom. The local directions of resolved tensile and compressive stresses are indicated.

coating materials under a static load of $P_{max}(=35\,kN)$ prior to the fatigue test. The more sensitive of these coatings cracked after only 5×10^3 cycles, whilst the third coating cracked, due to local tensile stresses after some 150×10^3 cycles. Because the coatings had been bonded to the I-beam it was not feasible to X-ray the specimen after the 3.11×10^6 cycles of the fatigue test. Consequently, it was considered that SEM might reveal characteristic fractographic features around the large web notch, where the fatigue damage was concentrated. However, this was unsuccessful because dye penetrant, that had been used for X-radiography, masked the features on the fracture surfaces. Therefore, the only quantitative damage results that have been obtained are those associated with the first notched glass/epoxy I-beam.

Tensile damage has been identified in two quadrants around the large notch. This was apparent visually and ultrasonically but was not fully identified using X-radiography, as shown in Fig. 9. Indeed, it was more difficult to identify the extent of damage within the glass/epoxy beams than within the carbon/epoxy beams when examining the through-thickness damage using optical microscopy. This is due to the lack of contrast obtained between the damage and glass/epoxy system when compared with the high contrast obtained between the damage and the carbon/epoxy system. However, no damage in the two compressive quadrants was identified in the glass/epoxy I-beams.

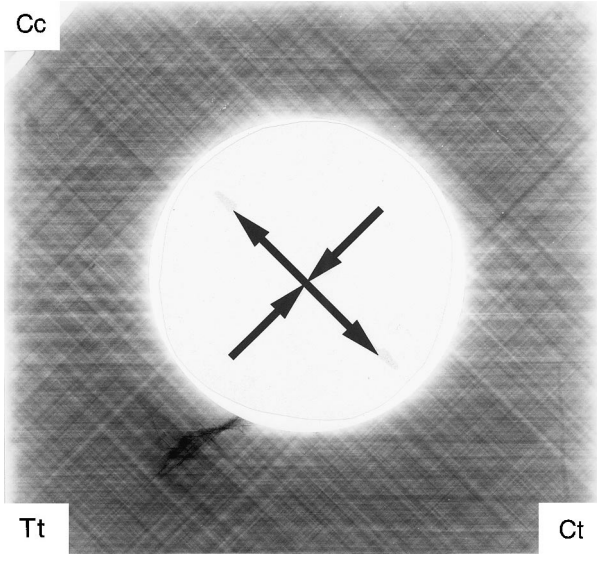

Fig. 9. X-ray radiograph of fatigue damage around 60 mm diameter notch in beam Glass N1 (0.96×10^6 cycles). Tensile damage, in the form of matrix cracks and delamination, exists in the two tensile quadrants Tc and Tt (top right and bottom left) although the damage is only visible in quadrant Tt (bottom left). The compression flange is along the top of the photograph and the tension flange along the bottom. The local directions of resolved tensile and compressive stresses are indicated.

3.4. Summary

No fatigue damage occurred in either the unnotched carbon/epoxy or the unnotched glass/epoxy I-beams. However, extensive tensile and compressive-induced damage initiated and developed around the circular web notches in the notched I-beams. Within the notched carbon/epoxy I-beams, tensile matrix cracks initiated quickly during the fatigue tests and propagated radially outwards from the edge of the notches. Delamination also occurred, but this was mainly limited to the compressive quadrants at the edge of the notches. Local tensile stresses eventually led to fibre fracture, and fracture of the fibres was the final cause of structural failure. Damage within the notched glass/epoxy I-beams, on the other hand, was less extensive and, whilst no glass/epoxy beam was fatigued to failure, all the damage was limited to the tensile quadrants around the notches. Matrix cracking and some delamination were observed.

The notched beam Carbon N5 failed after being fatigued for 4.78×10^6 cycles at a load ratio of 0.1. Failure was confined to the web region containing the large notch. None of the notched glass beams were fatigued to catastrophic failure although beam Glass N2, also tested at a load ratio of 0.1 for 3.11×10^6 cycles, contained damage within the web region around the large notch.

4. Discussion

4.1. Introduction

The general mechanisms of damage that occurred within the carbon/epoxy and glass/epoxy beam tests have been described in the previous sections. These have been quantified in three dimensions for the various I-beams using X-radiography, ultrasonics, edge replication and optical microscopy. The present section discusses the development of the damage mechanisms through the thickness of the beam with respect to ply orientation, fatigue cycles, and distance from the edge of the large web notches. Since damage and failure of the notched I-beams were localised around the large web notch it is this region of the I-beams that has been investigated in most detail. Similarly, since more carbon/epoxy beams have been tested than glass/epoxy beams, it is the development of damage within the carbon beams that is discussed in this section.

The damage around the notches in the web regions of the I-beams, shown variously in Figs. 3, 5 and 6, was located in four different quadrants, identified as Tt, Tc, Cc and Ct, which were defined by the nature of the resolved stresses in the shear loaded web regions. The resolved stress state in diagonally opposite quadrants is either compressive or tensile. Two quadrants are

adjacent to the tension flange while the other two are adjacent to the compression flange. The notation used in the present work to define these four quadrants specifies both the resolved stress state and the flange which is adjacent to the particular quadrant. For example, the stress state in quadrant Tt is resolved tension and this quadrant is adjacent to the tension flange. Quadrant Ct, on the other hand, is subject to resolved compressive stress and is adjacent to the tension flange.

4.2. Matrix cracking

The extent of matrix cracking throughout the notched regions of the various I-beams was most readily quantified using optical microscopy to examine a series of sections taken from around the 60 mm diameter notches. Such microscopy sections were typically 20 mm wide and the different densities of matrix cracks (defined by the number of cracks per mm in a given ply) were calculated by visually counting every matrix crack in each ply of each section and normalising against the width of the particular microscopy section. It is important to note, however, that there are practical difficulties associated with distinguishing between matrix cracks, polishing scratches, regions of resin richness or sparseness and shadows, and consequently there is an element of scatter in the number of cracks that were counted in each ply. It is estimated that this error in determining the value of matrix crack density is approximately $\pm 10\%$.

Sections were taken tangential to the hole and at distances up to 25 mm away from the edge of the 60 mm diameter notch in the two tensile quadrants. The sections within particular quadrants were all nominally parallel to each other and oriented parallel to the diagonal tension within the particular quadrants. This is shown schematically in Fig. 2. It should be noted that this is a consequence of the fact that the orientation of these microscopy sections is rotated through 45°, with respect to the reference system that has been used to define the stacking sequence in the beams (i.e. the global coordinate system). Namely, the various plies of the microscopy sections, such as Fig. 7, do not have the same visual appearance as the globally defined stacking sequence. In other words, the global stacking sequence of $(+45/0/-45°)_{2s}(-45/0/+45°)_{2s}$ identified in Fig. 1 and in Section 2.1 appears locally as:

$$0/-45/90/0/-45/90/90/-45/0/90/-45/0/90/-45/0/90/-45/0/0/-45/90/0/-45/90°.$$

The significance of this is that fibres within the local 90° plies are the ones which are normal to the resolved tensile stresses that exists within quadrants Tt and Tc.

Fig. 10(a–d) and Fig. 11(a–d) quantify, for quadrants Tt and Tc, respectively, the density of matrix cracking

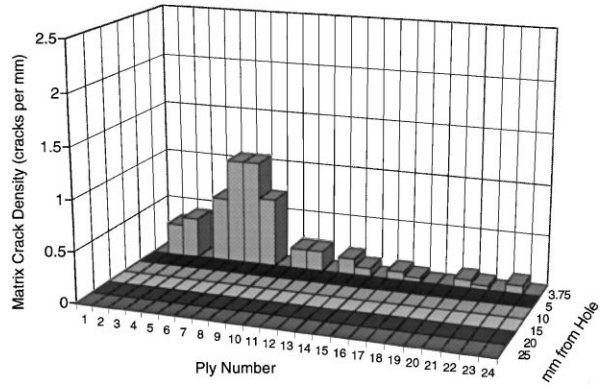

Fig. 10. (a) Density of matrix cracking in quadrant Tt of beam Carbon N2 after 0.5×10^6 cycles. The damage in each of the 24 plies at different distances ahead of the edge of the 60 mm diameter notch is identified. The local orientation of plies 1–24 is $(0/-45/90°)_{2s}(90/-45/0°)_{2s}$, respectively.

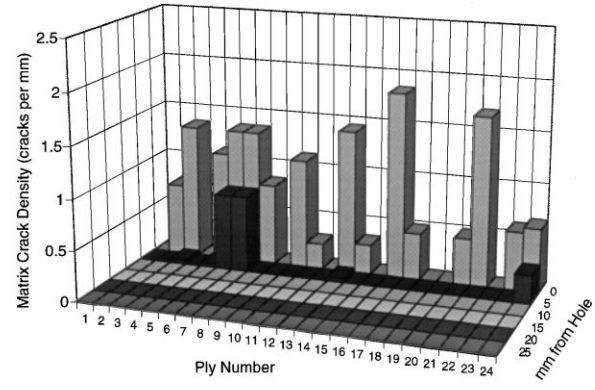

Fig. 10. (b) Density of matrix cracking in quadrant Tt of beam Carbon N3 after 2.43×10^6 cycles. The damage in each of the 24 plies at different distances ahead of the edge of the 60 mm diameter notch is identified. The local orientation of plies 1–24 is $(0/-45/90°)_{2s}(90/-45/0°)_{2s}$, respectively.

(number of cracks per mm) in each of the 24 plies at different distances away from the edge of the large web notch at 0.5×10^6, 2.43×10^6, 4.5×10^6 and 4.78×10^6 cycles (i.e. specimens cut from carbon beams N2 to N5, respectively). Tensile stress exists in these two quadrants due to the resolved shear stresses in this web region of the I-beams; quadrant Tt is adjacent to the tensile flange of the I-beams whilst quadrant Tc is adjacent to the compressive flange, and hence the overall stress state differs in the two quadrants. Firstly, it may be seen that the density of matrix cracking in the quadrant Tt is consistently somewhat greater than in quadrant Tc around the notch. Secondly, no matrix cracks were seen in the local 0° plies because microscopy sections were taken parallel to the fibres. However, some matrix fracture in the local 0° plies did actually occur. This can be seen in the X-radiographs of Fig. 6(a–d), although a close inspection of these radiographs indicate that the

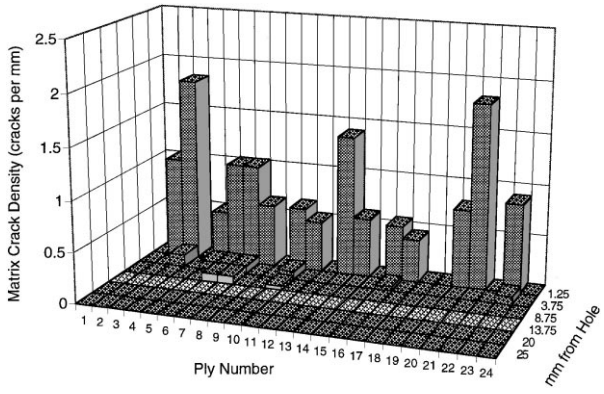

Fig. 10. (c) Density of matrix cracking in quadrant Tt of beam Carbon N4 after 4.5×10^6 cycles. The damage in each of the 24 plies at different distances ahead of the edge of the 60 mm diameter notch is identified. The local orientation of plies 1–24 is $(0/-45/90°)_{2s}(90/-45/0°)_{2s}$, respectively.

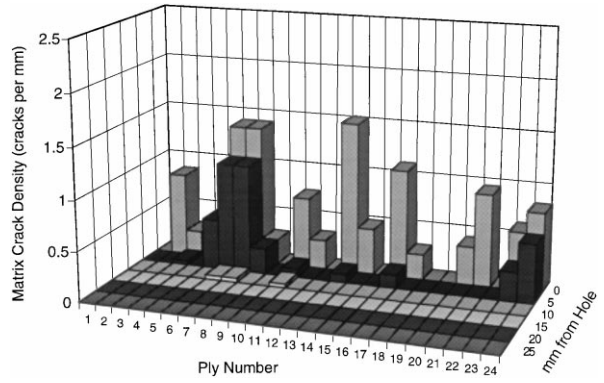

Fig. 11. (b) Density of matrix cracking in quadrant Tc of beam Carbon N3 after 2.43×10^6 cycles. The damage in each of the 24 plies at different distances ahead of the edge of the 60 mm diameter notch is identified. The local orientation of plies 1–24 is $(0/-45/90°)_{2s}(90/-45/0°)_{2s}$, respectively.

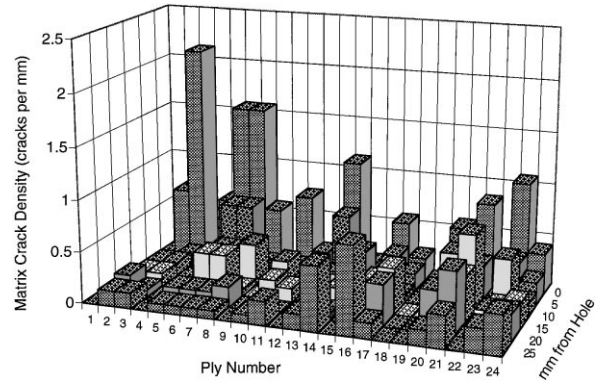

Fig. 10. (d) Density of matrix cracking in quadrant Tt of beam Carbon N5 after 4.78×10^6 cycles. The damage in each of the 24 plies at different distances ahead of the edge of the 60 mm diameter notch is identified. The local orientation of plies 1–24 is $(0/-45/90°)_{2s}(90/-45/0°)_{2s}$, respectively.

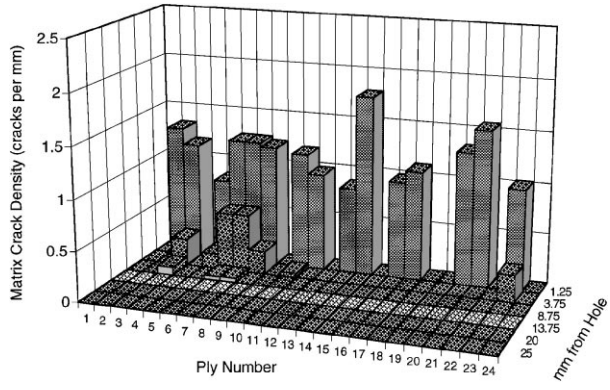

Fig. 11. (c) Density of matrix cracking in quadrant Tc of beam Carbon N4 after 4.5×10^6 cycles. The damage in each of the 24 plies at different distances ahead of the edge of the 60 mm diameter notch is identified. The local orientation of plies 1–24 is $(0/-45/90°)_{2s}(90/-45/0°)_{2s}$, respectively.

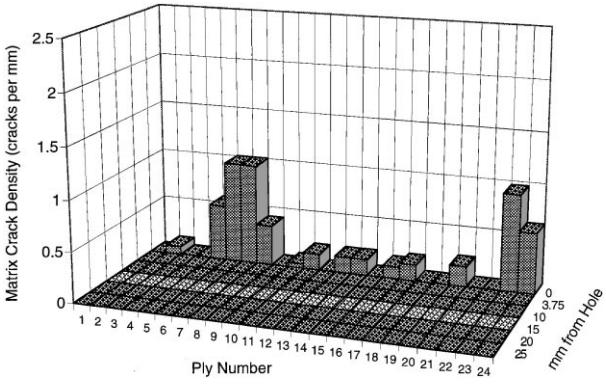

Fig. 11. (a) Density of matrix cracking in quadrant Tc of beam Carbon N2 after 0.5×10^6 cycles. The damage in each of the 24 plies at different distances ahead of the edge of the 60 mm diameter notch is identified. The local orientation of plies 1–24 is $(0/-45/90°)_{2s}(90/-45/0°)_{2s}$, respectively.

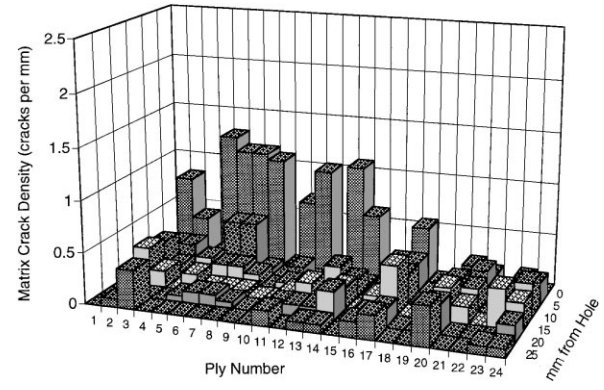

Fig. 11. (d) Density of matrix cracking in quadrant Tc of beam Carbon N5 after 4.78×10^6 cycles. The damage in each of the 24 plies at different distances ahead of the edge of the 60 mm diameter notch is identified. The local orientation of plies 1–24 is $(0/-45/90°)_{2s}(90/-45/0°)_{2s}$, respectively.

local 0° ply matrix damage is associated with delamination of surface plies as a result of machining the web notches. Such damage does not extend beyond the immediate area of the holes and consequently, it was not considered necessary to section the optical microscopy specimens at different orientations in order to detect damage in local 0° plies.

Subsequent analysis of the results presented in Fig. 10(a–d) and Fig. 11(a–d) gives the average matrix crack density in plies of −45 and 90° local orientations, and this is shown in Fig. 12(a–d) and Fig. 13(a–d). This conveniently reveals the propensity for matrix cracking to occur in plies of particular orientations when subjected to local tensile stress. The 90° plies merit further classification into single 90° plies, of which there are six through the thickness of the beams, and double 90° plies, of which there is one through the thickness of the beams. Such further analysis reveals that there is a greater inclination for matrix cracking to occur in the double 90° plies than in the single 90° plies. The extent to which there is a greater density of matrix cracking in the local double 90° plies than in the local single 90°

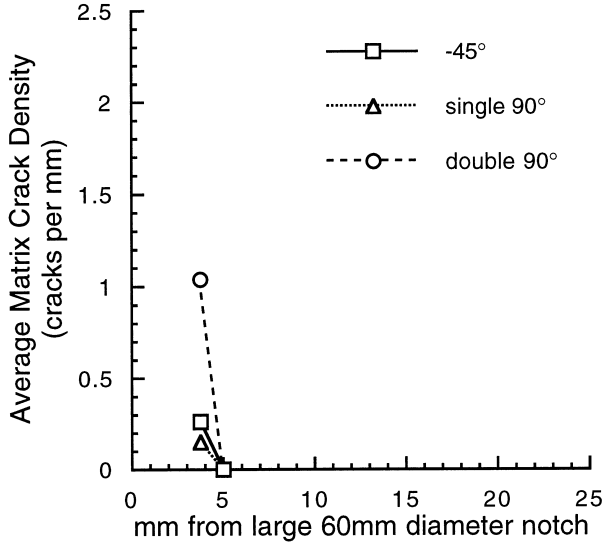

Fig. 12. (a) Average density of matrix cracking in quadrant Tt of beam Carbon N2 after 0.5×10^6 cycles. The average damage in locally oriented −45° plies, single 90° plies and double 90° plies is identified at different distances ahead of the edge of the 60 mm diameter notch.

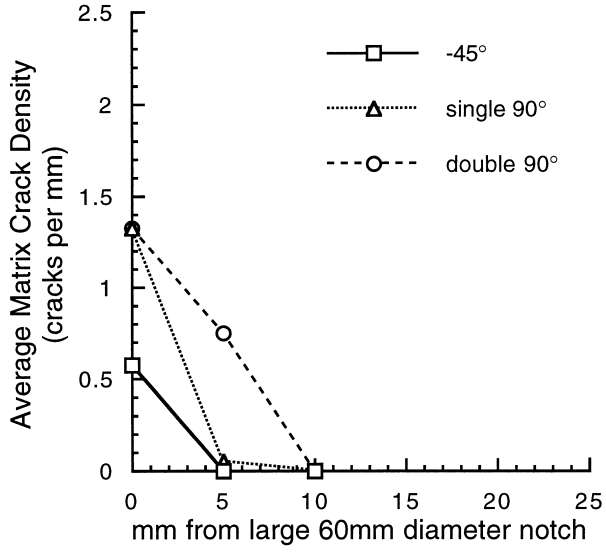

Fig. 12. (b) Average density of matrix cracking in quadrant Tt of beam Carbon N3 after 2.43×10^6 cycles. The average damage in locally oriented −45° plies, single 90° plies and double 90° plies is identified at different distances ahead of the edge of the 60 mm diameter notch.

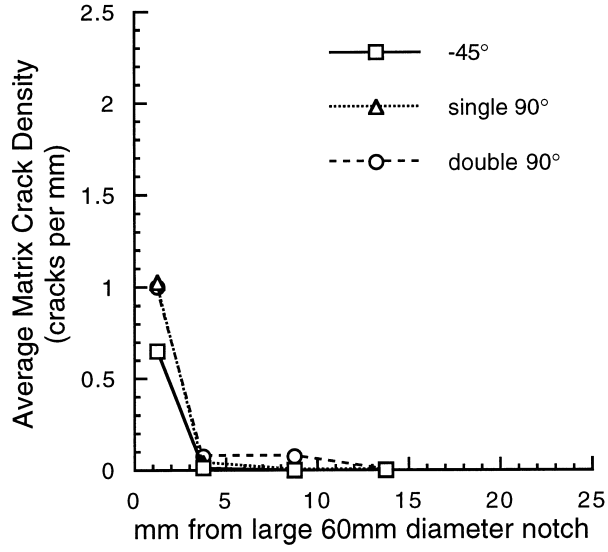

Fig. 12. (c) Average density of matrix cracking in quadrant Tt of beam Carbon N4 after 4.5×10^6 cycles. The average damage in locally oriented −45° plies, single 90° plies and double 90° plies is identified at different distances ahead of the edge of the 60 mm diameter notch.

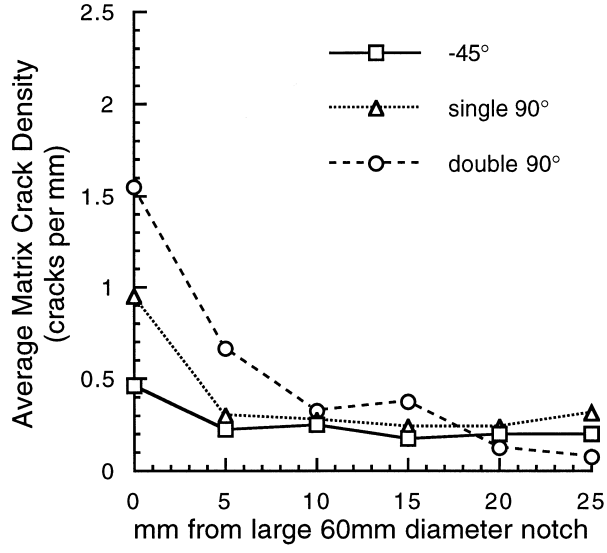

Fig. 12. (d) Average density of matrix cracking in quadrant Tt of beam Carbon N5 after 4.78×10^6 cycles. The average damage in locally oriented −45° plies, single 90° plies and double 90° plies is identified at different distances ahead of the edge of the 60 mm diameter notch.

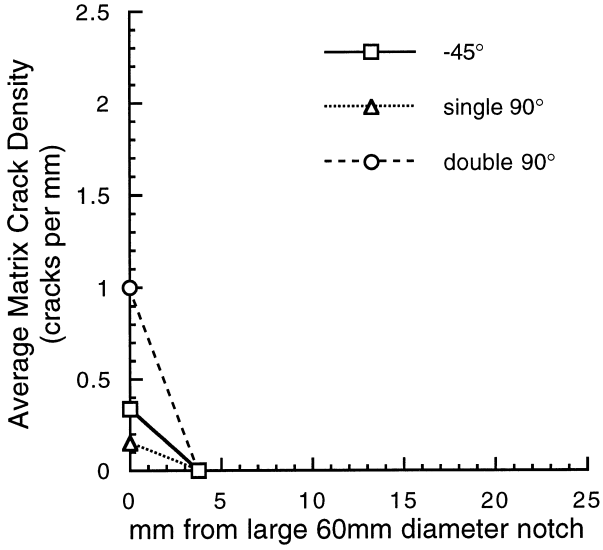

Fig. 13. (a) Average density of matrix cracking in quadrant Tc of beam Carbon N2 after 0.5×10^6 cycles. The average damage in locally oriented −45° plies, single 90° plies and double 90° plies is identified at different distances ahead of the edge of the 60 mm diameter notch.

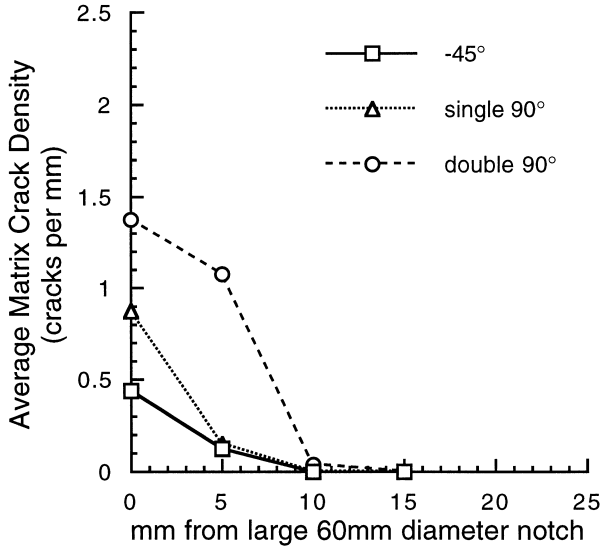

Fig. 13. (b) Average density of matrix cracking in quadrant Tc of beam Carbon N3 after 2.43×10^6 cycles. The average damage in locally oriented −45° plies, single 90° plies and double 90° plies is identified at different distances ahead of the edge of the 60 mm diameter notch.

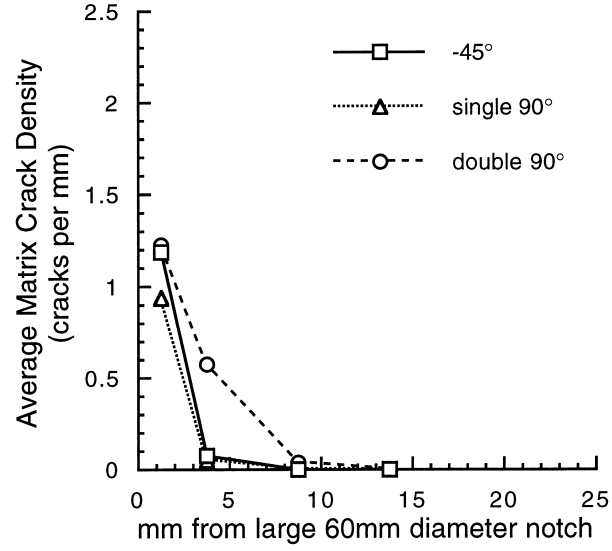

Fig. 13. (c) Average density of matrix cracking in quadrant Tc of beam Carbon N4 after 4.5×10^6 cycles. The average damage in locally oriented −45° plies, single 90° plies and double 90° plies is identified at different distances ahead of the edge of the 60 mm diameter notch.

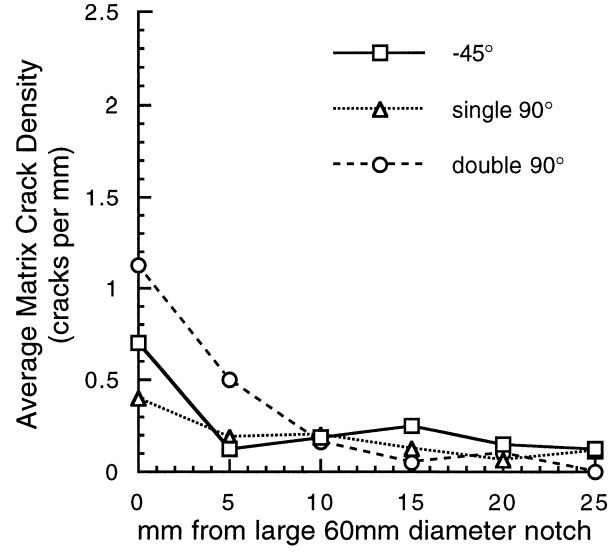

Fig. 13. (d) Average density of matrix cracking in quadrant Tc of beam Carbon N5 after 4.78×10^6 cycles. The average damage in locally oriented −45° plies, single 90° plies and double 90° plies is identified at different distances ahead of the edge of the 60 mm diameter notch.

plies varies in a relatively consistent manner and depends on whether the section is from quadrant Tt or Tc, on how far the section is from the edge of the hole and on the number of fatigue cycles. It is believed that the lower density of matrix cracking in the single 90° plies is due to the greater constraint provided by adjacent 0 and −45° plies, which are closer to the centre of a single 90° ply than the centre of a double 90° ply.

It is not possible to accurately quantify the relative differences in matrix crack density at distinct distances from the notch in both quadrants Tt and Tc at different numbers of fatigue cycles. However, of the three different ply orientations, the greatest density of matrix cracking existed in the double 90° plies whilst there was the least amount of matrix cracking in the −45° plies. It is also clear that the −45°, the single 90° and the double 90° plies all contained matrix cracks within the first 0.5×10^6 cycles of fatigue loading. There has also been a slightly greater tendency for matrix cracking to occur in the Tt quadrant compared with quadrant Tc around the notch.

It is difficult to quantify the rate at which the average matrix crack density evolved at different distances from the edge of the web notch with respect to the number of fatigue cycles. This is due in part to the fact that the optical micrographs could not be consistently taken at identical distances from the edge of the notch and partly to the difficulties associated with precisely identifying matrix cracks. The fact that such a comparison is being made between different I-beam specimens, which were albeit tested under nominally identical conditions, compounded the difficulties in quantifying the rate of damage development with fatigue cycles. Nevertheless, it has been possible to estimate the evolution rate of matrix cracking. Figs. 12–14 detail the average matrix crack density in the double 90° ply, the single 90° plies and the −45° plies at different distances away from the edge of the notch in quadrants Tt and Tc for different numbers of fatigue cycles. Close examination of these data, comparing between the same distances from the edge of the notches across beam tests (i.e. for different numbers of fatigue cycles), indicates that the density of matrix cracking increases in a non-linear manner with fatigue cycles. In particular, the matrix crack density increased most rapidly during the first interval of fatigue loading, i.e. between zero and 0.5×10^6 cycles, after which there was a more gradual increase in the density of matrix cracking. As noted above, the plies that exhibited most matrix cracking were the local double 90° plies, with the local −45° plies exhibiting far fewer matrix cracks than the local single 90° plies. The density of matrix cracking in both the local double 90° and local single 90° plies typically reached levels of between 1–1.5 cracks/mm and did not exceed this level. This density of cracking is lower than the characteristic damage state that is commonly cited [40] as being reached prior to fatigue fracture, i.e. levels between 4 to 16 matrix cracks/mm ($\approx$ 0.5 and 2.0 matrix cracks per ply thickness), depending on the particular stacking sequence.

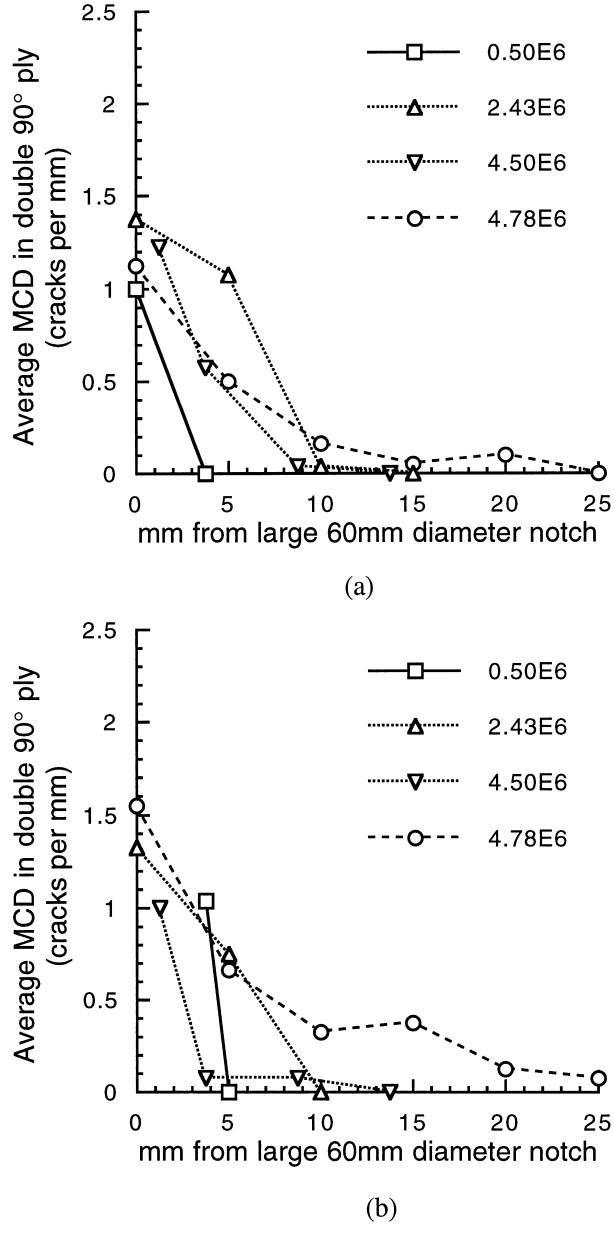

Fig. 14. Average density of matrix cracking in local double 90° plies (a) in quadrants Tc and (b) in quadrants Tt. The average damage is identified at different distances ahead of the edge of the 60 mm diameter notch and at different numbers of fatigue cycles.

4.3. Fibre fracture

The through-thickness optical micrographs that have been analysed in the preceding section to examine matrix cracking were also examined to identify the extent of fibre fracture throughout the web-notched regions of the carbon/epoxy I-beams. Whilst the particular micrographs of Fig. 7 reveal matrix cracks in local −45 and 90° plies, they do not reveal any fibre fracture, although the detection of fibre fracture would depend upon the orientation of a particular microscopy section.

However, a small amount of fibre fracture was detected in some of the local 0° plies adjacent to the edge of the large web hole after only 0.5×10^6 cycles. Out of some eighteen fibres in the thickness of a single ply, there were two fractured fibres in only one of the eight 0° plies. This small amount of fibre fracture was also present close to the edge of the hole after 2.43×10^6 cycles, and after 4.5×10^6 cycles a similar amount was also present at a distance of almost 10 mm away from the edge of the hole. Consequently, it is possible that both matrix cracking and fibre fracture within the Tt quadrant (i.e. the quadrant subject to local tensile stress conditions adjacent to the tensile flange) attain some critical level prior to catastrophic fracture.

After 4.78×10^6 cycles, the web region around the large notch in beam Carbon N5 failed with extensive fibre fracture being present from the edge of the notch to the tensile and compressive flanges (see Fig. 8). This

led to a through-thickness crack growing at right angles to the local tensile stresses through the web until it met the compressive and tensile flanges, again as may be seen in Fig. 8. This resulted in structural failure of the I-beam.

4.4. Delamination

Extensive delamination occurred within quadrant Cc (i.e. the area subjected to local compressive stresses adjacent to the compression flange) after only 0.5×10^6 cycles. The X-radiographs of Fig. 6(a–c) indicate that some delamination also occurred in the other three quadrants. However, the delaminations in these other quadrants were exclusively associated with damage to surface plies when initially machining the holes, and these delaminations did not extend outwards from the edges of the notches. Delamination within quadrant Cc, on the other hand, occurred along almost all of the local $-45/90^\circ$ and $90/0^\circ$ interfaces with negligible delamination along the $0/-45^\circ$ interfaces.

During the initial stages of fatigue testing, prior to the development of delamination, there was no web buckling around the holes. This was as expected, since the maximum fatigue load was less than that required to cause buckling. However, local web buckling occurred around the circumference of the large web notches (i.e. the 60 mm diameter holes) once delamination had occurred. The plies on either side of the delamination were visually seen to buckle in-phase with the frequency of the fatigue load, and at failure the delamination extended radially outwards from the edge of the hole to the diagonal corner of the web adjacent to the compressive flange, i.e. quadrant Cc. The width of the delamination, seen typically in the X-ray of Fig. 6(c), was of the same order as the diameter of the notch. Table 5 identifies the increase with delamination area in quadrant Cc as a function of fatigue cycles. These approximate measures of area have been taken from the X-radiographs of Fig. 6(a–c) and they identify the almost negligible growth in delamination until catastrophic failure. (These measures of delaminated area are per unit area of beam surface as would be detected using ultrasonic C-scan, and are not per unit interface within an area of beam surface.)

Table 5
Approximate area of delamination in quadrant Cc round the 60 mm diameter notch as a function of number of fatigue cycles, N (measured from X-radiographs of Fig. 6)

$N\times10^6$ cycles	Delamination area (mm^2)
0	0
0.5	7
4.5	198
4.78	2150

4.5. Sequence of damage and failure

By considering the evidence of the damage that occurred in the five notched carbon beams it is possible to suggest a likely sequence of damage events that led to ultimate fracture. Within quadrants Tt and Tc, which were subjected to resolved tensile stresses, matrix cracking occurred in plies of -45 and 90° local orientations within 0.5×10^6 cycles. It is not known which plies cracked first although it is likely that local 90° plies were the first to suffer matrix cracks; the matrix cracking in these plies was certainly more dense, more extensive and present at distances further from the web notch than in other plies.

The matrix cracking in the local double 90° plies was usually somewhat greater than in the local single 90° plies, and it is believed that the smaller constraint afforded by adjacent plies on the double 90° plies, than on the single 90° plies, permitted the matrix cracks in the double 90° plies to propagate furthest from the edge of the web notch in any given number of fatigue cycles. In any event, at fracture, i.e. after 4.78×10^6 cycles for beam Carbon N5, both the matrix and the fibres of all 24 plies had failed completely in quadrants Tt and Tc between the hole and the tensile and compressive flanges. The rate at which matrix cracking occurred in the local 90° plies is reasonably clear from the X-radiography evidence: an initially relatively fast rate of cracking (within the first 0.5×10^6 cycles) occurred, which then slowed down for the bulk of the fatigue life (from 0.5 to 4.5×10^6 cycles), and finally accelerated rapidly (within tens of thousands of cycles) before failure.

The rate of damage evolution has been described qualitatively from the ultrasonic C-scans and the X-radiographs of Figs. 3, 5 and 6, and to some extent quantitatively in Figs. 10–14. The matrix cracking in the local 90° plies is believed to be the critical damage mechanism that leads to fibre fracture and, hence, ultimate failure of the web region of the carbon beams. The preceding X-radiographic evidence can be analysed further to relate the area of matrix damage in the local 90° plies with the number of fatigue cycles, as shown in Fig. 15. These results have been calculated directly from the X-radiographs of Fig. 6(a–c) by measuring the areas of matrix cracking in single and double 90° plies around the large holes. (It is important to note that these data do not distinguish between single and double 90° plies and are given in terms of per unit area of beam surface.) By examining Fig. 15 it is possible to obtain some indicative estimates of the growth rate damage area in the single and double local 90° plies with the number of fatigue cycles. The slopes of the various stages of damage development in Fig. 15 indicate that the initial and final stages of growth were almost an order of magnitude faster than that of the intermediate stage.

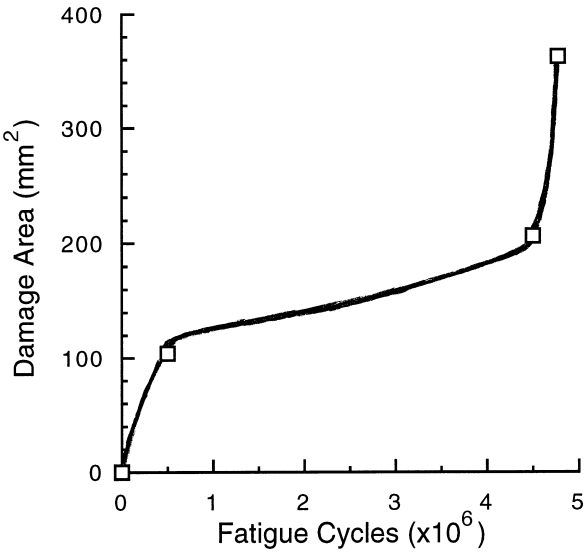

Fig. 15. Approximate area of matrix cracking in local single 90° plies and double 90° plies around the 60 mm diameter notch (average of quadrants Tt and Tc) as a function of the number of fatigue cycles.

Within quadrants Cc and Ct, on the other hand, which were subjected to resolved compressive stresses, some delamination of surface plies occurred close to the 60 mm diameter web notch. The propagation of the delaminations in quadrant Ct may have been due to the initial poor quality of the machined notch, but delaminations developed in quadrant Cc irrespective of the quality of the machining operation. The rate of delamination growth in quadrant Cc was possibly assisted by the fact that the maximum fatigue load (P_{max}) was close to the load at which web buckling would occur in the undamaged beams; indeed the delaminated region in quadrant Cc 'panted open and closed' with each fatigue cycle. However, at final failure (i.e. after 4.78×10^6 cycles for beam N5) delamination was not present in quadrant Ct and was only present in quadrant Cc. This delamination in quadrant Cc extended from the hole to the flange and was approximately as wide as the diameter of the notch. The increase in the area of delamination in quadrant Cc around the 60 mm diameter notch is given in Table 5 and shows that very little delamination occurred until the number of cycles was relatively high. It is suspected that the extensive development of delamination close to failure is a consequence of the tensile fracture in quadrants Tt and Tc.

5. Conclusions

The present paper is the third in a series which is concerned with the static and cyclic fatigue failure of composite I-beams. Both carbon-fibre/epoxy-matrix and glass-fibre/epoxy-matrix composites have been used to manufacture the I-beams, which had a multi-directional stacking sequence consisting of a balanced layup of 0, +45 and −45° plies. Both unnotched and notched I-beams have been studied. A four-point flexural configuration has been used to test the I-beams and in no cases were the beams fatigued above the loads at which buckling of the compression flanges occurred during static testing.

The carbon/epoxy and glass/epoxy I-beams which were unnotched did not exhibit any detectable damage within 1.2×10^6 and 8×10^6 fatigue cycles, respectively. At these numbers of cycles the fatigue tests were halted. The excellent fatigue behaviour of these unnotched composite I-beams is most noteworthy, especially since the maximum fatigue loads which were applied represented typically about 75 to 100% of the loads needed to cause buckling of the compression flange during static testing.

Hence, the I-beams were notched in order to induce failure under the fatigue loads. The most damaging type of notch that was introduced was a 60 mm diameter hole in the web section of the I-beam (see Fig. 2). The notched I-beams now did indeed fail under the fatigue loads. For example, in the case of the carbon-fibre/epoxy-matrix I-beams which were fatigue loaded at 5 Hz from 5 kN to 50 kN (which represented about 9 to 90% of the load at which buckling of the compression flanges occurred during static testing) failed after 4.78×10^6 cycles. Fatigue failure was due to various types of damage, including delamination, matrix microcracking and fibre fracture, occurring around the 60 mm diameter web notch.

The damage mechanisms in the notched carbon-fibre/epoxy-matrix I-beams were studied in detail. The most severe of such damage was caused by the tensile stresses which were present around the web notch. The principal mode of damage was matrix cracking, in plies oriented at 90° to the local direct tensile stress. A significant proportion of this damage occurred within the first 0.5×10^6 cycles. The matrix cracking led eventually to delamination and fibre fracture, the latter being the final cause of structural failure of the I-beam.

Acknowledgements

The authors acknowledge the financial assistance of British Aerospace plc, the DTI (via the LINK 'Structural Composites' programme), EI Du Pont de Nemours & Co. Inc., Rolls Royce plc, the SERC (now EPSRC), Shell Research and Westland Helicopters Ltd. as well as the advice of Professor P. Curtis of DRA, Farnborough. The assistance of Mr E. W. Godwin and Mr H.J. MacGillivray, of Imperial College, throughout this project is acknowledged. The authors would also like to thank Mr. E.W. O'Brien of British Aerospace

plc, Filton, for his assistance with photoelastic coatings, and the EPSRC for providing thermal imaging equipment.

References

[1] Chandra R, Chopra I. Experimental and theoretical analysis of composite I beams with elastic couplings. AIAA Journal 1991;29:2197–206.

[2] Hollmann K. Failure analysis of a shear loaded graphite/epoxy beam containing an irregular cutout. Engng Fract Mechs 1991;39:159–75.

[3] Smith SJ, Bank LC. Modifications to beam theory for bending and twisting of open-section composite beams—experimental verification. Composite Structures 1992;22:169–77.

[4] Purslow D. Composites fractography without an SEM—the failure analysis of a CFRP I beam. Composites 1984;15:43–8.

[5] Kedward KT, Wilson RS, McLean SK. Flexure of simply curved composite shapes. Composites 1989;20:527–36.

[6] Greenhalgh ES. Mechanical evaluation of carbon-fibre reinforced thermoplastic I beams, DRA TR 92071, Farnborough, UK, 1993.

[7] Takayanagi H, Kemmochi K, Sembokuya H, Hojo M, Maki H. Shear-lag effect in CFRP I beams under three-point bending. Experimental Mechanics 1994; June:100–7.

[8] Mandell JF, Meier U. Effects of stress ratio, frequency and loading time on the tensile fatigue of glass-reinforced epoxy. In: O'Brien TK, editor. Long-term behaviour of composites. ASTM STP 813. Philadelphia (PA):American Society for Testing and Materials, 1983. p. 55–77.

[9] Meier U, Mueller R, Puck A. FRP-box beams under static and fatigue loading. In: Feest T, editor. Proc. of the Int. Conf. on Testing, Evaluation and Quality Control of Composites, TEQC83. Surrey University, Guildford, UK, 13–14 September. 1983. p. 324–36

[10] Gilchrist MD, Kinloch AJ, Matthews FL, Osiyemi SO. Mechanical performance of carbon-fibre- and glass-fibre-reinforced epoxy I beams: I. Mechanical behaviour. Comp Sci Technol 1996;56:37–53.

[11] Gilchrist MD, Kinloch AJ, Matthews FL. Mechanical performance of carbon-fibre- and glass-fibre-reinforced epoxy I beams: II. Fractographic failure observations. Comp Sci Technol 1996;56:1031–45.

[12] Allen HG, Bulson PS. Background to buckling. New York: McGraw Hill, 1980.

[13] Mottram JT. Structural properties of a pultruded E-glass fibre-reinforced polymeric I beam. In: Marshall IH, editor. Proc. 6th Int. Conf. Composite Structures, Paisley, UK: Elsevier Applied Science, 9–11 September, 1991. p. 1–28.

[14] Mottram JT. Evaluation of design analysis for pultruded fibre-reinforced polymeric box beams. The Structural Engineer 1991;69(11):211–20.

[15] Mottram JT. Lateral-torsional buckling of a pultruded I beam. Composites 1992;23:81–92.

[16] Mottram JT. Lateral-torsional buckling of thin-walled composite I beams by the finite difference method. Composites Engineering 1992;2:91–104.

[17] Miller AG, Wingert AL. Fracture surface characterization of commercial graphite/epoxy systems. In: Pipes RB, editor. Nondestructive Evaluation and Flaw Criticality for Composite Materials. ASTM STP 696. Philadelphia (PA): American Society for Testing and Materials, 1979. p. 223–73.

[18] Morris GE. Determining fracture directions and fracture origins on failed graphite/epoxy surfaces. In: Pipes RB, editor. Nondestructive Evaluation and Flaw Criticality for Composite Materials. ASTM STP 696. Philadelphia (PA): American Society for Testing and Materials, 1979. p 274–97.

[19] Purslow D. Some fundamental aspects of composites fractography. RAE TR 81127. Farnborough (UK): Royal Aircraft Establishment, October 1981.

[20] Purslow D. Matrix fractography of fibre-epoxy composites. RAE TR 86046. Farborough (UK): Royal Aircraft Establishment, July 1986.

[21] Zenkert D. Effect of manufacture-induced flaws on the strength of foam core sandwich beams. In: Masters JE, editor. Damage detection in composite materials. ASTM STP 1128. Philadelphia (PA): American Society for Testing and Materials, 1992. p. 137–51.

[22] Russell AJ, Street KN. The effect of matrix toughness on delamination: static and fatigue fracture under mode II shear loading of graphite fibre composites. In: Johnston NJ, editor. Toughened composites, ASTM STP 937. Philadelphia (PA): American Society for Testing and Materials, 1987. p. 275–94.

[23] Corberand PEL. Micromechanisms of mode II fatigue delamination in continuous fibre polymer composites. M.Sc. thesis, Cranfield Institute of Technology, UK, 1990.

[24] Franz HE. Characteristics of fatigue failures in fibre-reinforced plastics. RAE LT 2081. Farnborough (UK): Royal Aircraft Establishment, February, 1982.

[25] Morris GE, Hetter CM. Fractographic studies of graphite/epoxy fatigue specimens. In: Reifsnider KL, editor. Damage in composite materials, ASTM STP 775. Philadelphia (PA): American Society for Testing and Materials. 1982, p. 27–39.

[26] Scrivner GC, Chan WS. Effects of stress ratio on edge delamination characteristics in laminated composites. In: Stinchomb WW, Ashbaugh NE, editors, Composite materials: fatigue and fracture, vol. 4. ASTM STP 1156. Philadelphia (PA): American Society for Testing and Materials, 1993. p. 538–51.

[27] Henaff-Gardin C, Lafarie-Frenot MC. Fatigue behaviour of thermoset and thermoplastic cross-ply laminates. Composites 1992;23:109–16.

[28] Gilchrist MD, Svensson N. A fractographic analysis of delamination within multidirectional carbon/epoxy laminates. Comp Sci Technol 1995;55:195–207.

[29] Hiley MJ, Curtis PT. Mode II damage development in carbon fibre reinforced plastics. AGARD: 74th Structures and Materials Meeting, Patras, Greece, 1992.

[30] Chen AS, Harris B, Reiter H. The effect of fatigue damage on the mechanical properties of CFRP composites. Proc. ICCM8, SAMPE, Honolulu, August 1991.

[31] Chen AS, Harris B. Fatigue-induced damage mechanisms in carbon fibre-reinforced plastic composites. J Mat Sci 1993;28:2013–27.

[32] LAP: Laminate Analysis Program. Imperial College, London:-Centre for Composite Materials, 1991.

[33] Curtis PT., editor. CRAG test methods for the measurement of the engineering properties of fibre reinforced plastics. RAE TR 88012, Farnborough (UK): Royal Aircraft Establishment. 1988.

[34] Konishi D, Johnson W. Fatigue effects on delaminations and strength degradation in graphite/epoxy laminates. In: Composites materials: testing and design, ASTM STP 674. Philadelphia (PA): American Society for Testing and Materials, 1979. p. 597–619.

[35] Whitcomb J. Strain-energy release rate analysis of cyclic delamination growth in compressively loaded laminates. In: Wilkins D, editor. Effects of defects in composite materials, ASTM STP 836. Philadelphia (PA): American Society for Testing and Materials, 1984. p. 175–93.

[36] Russell AJ, Street KN. Predicting interlaminar fatigue crack growth rates in compressively loaded laminates. In: Legace P, editor. Composite materials: fatigue and fracture, vol. 2. ASTM STP 1012. Philadelphia (UK): American Society for Testing and Materials, 1989. p. 162–78.

[37] Kemmochi K, Uemura M. Measurement of stress distribution in sandwich beams under four-point bending. Exp Mechs 1980;20:80–6.
[38] Ahlstrom LM, Bäcklund J. Shape optimization of openings in composite pressure vessels. Comp Struct 1992;20:53–62.
[39] Kaczmarek H. Ultrasonic detection of the development of transverse cracking under monotonic tensile loading. Compos Sci Technol 1993;46:67–75.
[40] Highsmith AL, Reifsnider KL. Stiffness-reduction mechanisms in composite laminates. In: Reifsnider KL, editor. Damage in composite materials, ASTM STP 775. Philadelphia (PA): American Society for Testing and Materials, 1982. p. 103–17.

Notation

E	Young's modulus
G	Shear modulus
P	Load
R	Load ratio $= P_{min}/P_{max}$
SEM	Scanning electron microscopy
X	Strength
ν	Poisson's ratio
σ	Direct stress
τ	Shear stress

Subscripts

Lten	Longitudinal tensile
max	Maximum
mean	Mean ($= 1/2$(maximum + minimum))
min	Minimum
Tten	Transverse tensile
11	Longitudinal (unidirectional ply property)
22	Transverse (unidirectional ply property)